Spring 2014

EMI investigation and modeling of a flat panel display

Satyajeet Shinde

Department:

EMI INVESTIGATION AND MODELING OF A FLAT PANEL DISPLAY

by

SATYAJEET SHINDE

A THESIS

Presented to the Faculty of the Graduate School of the

MISSOURI UNIVERSITY OF SCIENCE AND TECHNOLOGY

In Partial Fulfillment of the Requirements for the Degree

MASTER OF SCIENCE IN ELECTRICAL ENGINEERING

2014

Approved by

David J. Pommerenke, Advisor
Jun Fan
Daryl G. Beetner

ABSTRACT

It is often important to carry out EMI analysis in the design phase of an electronic product to predict the radiated emissions. An EMI analysis is important to predict if the product complies with the FCC regulations as well as to gain an understanding of the noise coupling and radiation mechanisms. EMI analysis and prediction of radiated emissions in electronic products that have an electrically large chassis, pose a challenge due to the presence of multiple resonant structures and noise-coupling mechanisms.

The study focusses on the investigation of the main noise coupling mechanisms, the approach and methods used for the modeling of a flat panel display. Full-wave simulation models are a powerful tool for the prediction of radiated emissions and the visualization of coupling paths within the product. The first part deals with the measurement of radiated emissions from the display under standard test conditions and the identification of the main noise sources using near-field scanning. The contribution of the chassis components – frame, back cover and the back panel, to the radiated emission is analyzed using shielding measurements. Noise coupling from the main board, flex cables, display driver boards and the display is analyzed from measurements. The second part deals with the full-wave modeling of the components – main board, flex cables, chassis and the display driver boards. The modeling approach is demonstrated by highlighting some of the challenges in modeling larger structures having many details. The simulation model contains the main components of the TV that contribute to far-field radiation. The full-wave modeling is done using the CST Microwave Studio. Two sets of simulation models are described – the common mode models and the complete models. The use of the common mode models for the identification of the resonant structures is demonstrated. The far-field radiated emissions along with the coupling mechanism within the flat panel display can be predicted using the simulation model.

ACKNOWLEDGMENTS

I would like to express my sincere gratitude to Dr. David Pommerenke, my advisor, for his advice, instructions, and encouragement on my research work, financial support to my study and direction for this thesis during my pursuit of the Master's degree. I have learned countless things from him about the academic aspect of my research including all the theoretical and experimental knowledge and the skill for writing and presentation.

I would like to specially thank Dr. Jun Fan, Dr. Daryl Beetner and Dr. James Drewniak for their valuable advice and support on my research projects and thesis.

I would like to thank Kohei Masuda from Panasonic Corp. for his efforts and experience in building up the detailed simulation models and Xu Gao for his contribution in build-up and validation of some of the initial TV models.

I would also like to thank all other faculty members in EMC lab for teaching me in the classes and providing me with a great research environment. I would like to express my appreciation to all the students in the EMC lab for their teamwork. I am proud that I was a member of such an exceptional lab in EMC area.

Lastly, I am deeply grateful to my family and parents for their constant support and encouragement.

TABLE OF CONTENTS

LIST OF ILLUSTRATIONS

Page

1. INTRODUCTION

1.1. PROJECT MOTIVATION AND OBJECTIVE

It is often important to carry out EMI analysis in the design phase of an electronic product to predict the radiated emissions. An EMI analysis is important to predict if the product complies with the FCC regulations as well as to gain an understanding of the noise coupling and radiation mechanisms. EMI analysis and prediction of radiated emissions in electronic products that have an electrically large chassis, pose a challenge due to the presence of multiple resonant structures and noise-coupling mechanisms. EMI analysis of an LCD TV has shown presence of EMI antennas primarily consisting of shields that are not adequately bonded to one another [1]. Further is has been shown that the most significant source of EMI in the LCD monitor does not originate from the LCD panel itself but from the main PCB [1]. The usage of shielding techniques such as shielding cover and gaskets for reducing EMI has been demonstrated in [2]. Innovative PCB design for reducing EMI in TV main boards has been carried out in [3]. The analysis and techniques used for reducing EMI contribution due to the LCD /TFT display driver ICs and chip level EMI reducing techniques have been well studied in [4], [5], [6], [7], [8] and [9]. The study focusses on the investigation of the main noise coupling mechanisms, the approach and methods used for the modeling of a flat panel display. Full-wave simulation models are a powerful tool for the prediction of radiated emissions and the visualization of coupling paths within the product.

The motivation for this project is the prediction of the maximum emissions from an electronic product having an electrically large chassis using simulation models. This can help in understanding noise coupling mechanisms, identification of chassis antenna structures and shielding effects, gain understanding of the modeling path and methods for building up simulation models for such products and preventing potential EMC compliance failures by analysis using simulation models.

The objectives are the identification of noise coupling mechanisms within the chassis, demonstrate full-wave modeling approach of the TV components that contribute to radiated emissions, identification of resonant structures from the

common mode simulation models and analyze the effect of the chassis components on the radiation using the simulation model.

1.2. RESEARCH APPROACH

The research approach is divided into three main parts as shown in Figure 1.1. The first part deals with the analysis of the TV based on measurements. We begin the study by analysis of the radiated emissions from the TV. Possible radiating structures are identified by shielding certain regions of the TV and comparing the results with the baseline. Noise source identification is carried out by near-field scanning of the main board, flex cables, and display driver boards within the TV. Noise coupling from the different electronics parts to the chassis is analyzed along with the dominant coupling mechanisms. Resonant structures are identified by using a near-field scanning probe.

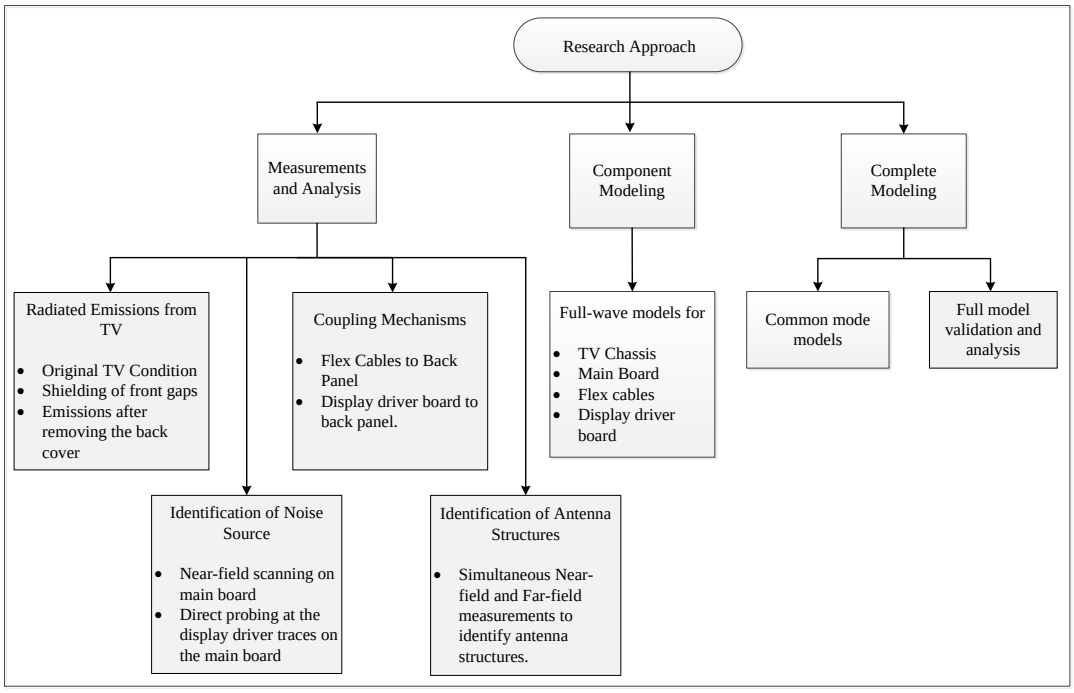

Figure 1.1. Research approach

2. MEASUREMENTS AND ANALYSIS

2.1. RADIATED EMISSIONS MEASUREMENTS

The objective of the baseline radiated emission test was to obtain the radiated emission of the TV with minimum configuration, and to observe the possible problematic frequencies. Figure 2.1 shows a typical 32-inch flat panel display.

Figure 2.1 Flat panel display

For the baseline measurement, radiated emission was measured in 3m semi-anechoic chamber. The receiver antenna was Sunol JB5 log periodic antenna, and it's vertical position was fixed at 1m for this initial testing. The horizontal position of the antenna was 3m away from the DUT. The DUT was placed on a 1m wooden table on a turntable, and the turntable was rotated from 0 to 360 degrees in 10 degree increments. For each turntable angle, the spectrum analyzer was set to max hold for approximately 25seconds (2600 sweeps). This time was determined by first observing when the max-hold data stabilizes. After going through all angles, the data was post processed to get the maximum over all angles for each frequency. The measurement was performed with vertical and horizontal polarization of the receiver antenna. Figure 2.3 shows the test setup.

During testing, the TV was only plugged into the power using the power cord supplied with the TV, and was displaying the following test image, as shown in Figure 2.2, loaded using a USB stick.

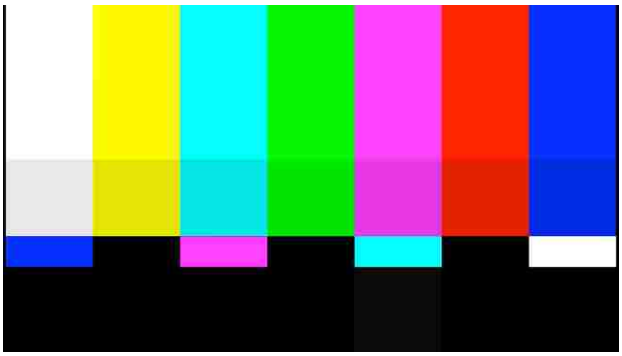

Figure 2.2. Test image displayed on the TV during radiated emission testing

Figure 2.3. Radiated emissions test setup

Also, the gain of the preamp and the loss of the cabling were measured and was taken into account in the post-processing of the data. Initially, the testing was

done at 30 -1000MHz frequency range, and later, the range was extended to 2GHz. Figure 2.4 shows the measurement setup.

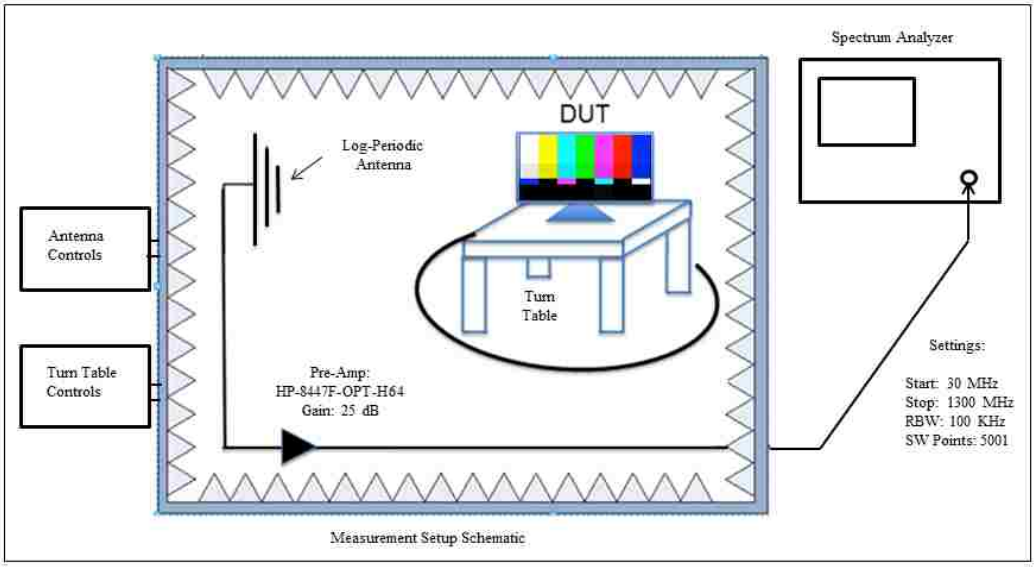

Figure 2.4. Measurement setup

Figure 2.5 shows the measured baseline radiated emissions. We focus on the signals caused by the LCD video data traffic.

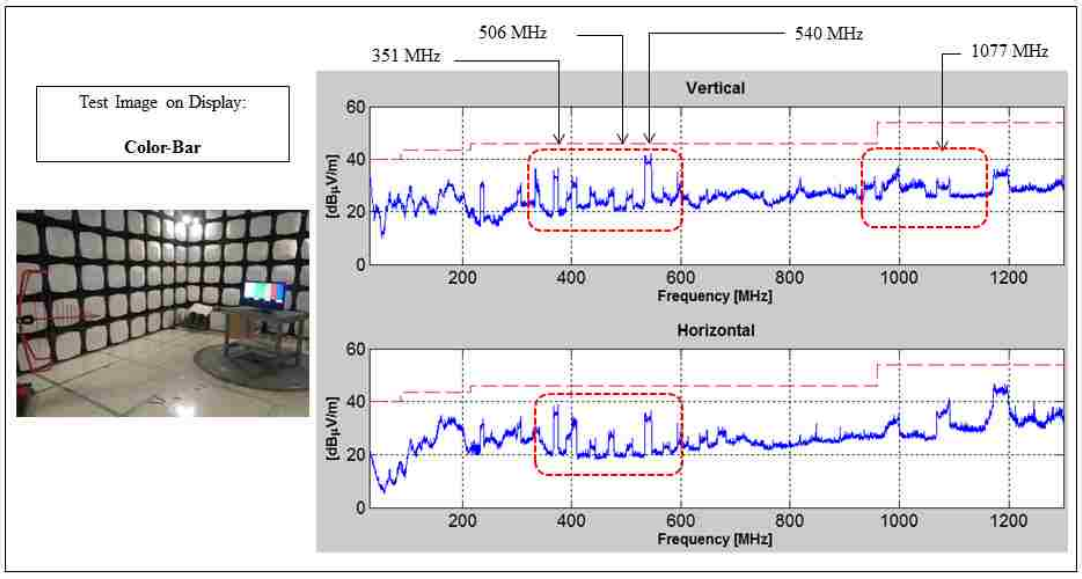

Figure 2.5. Baseline radiated emissions at 3m distance

The main components of the chassis are shown in Figure 2.6 for reference. The chassis consists of the following four components:

- Back Panel (Metallic)
- Back Cover (Metallic)
- Frame (Metallic)
- Dielectric spacer between frame and back panel. (a type of plastic material)
- Metallic Screws – **11** (connecting frame and back panel) and **9** (connecting back panel and back cover).

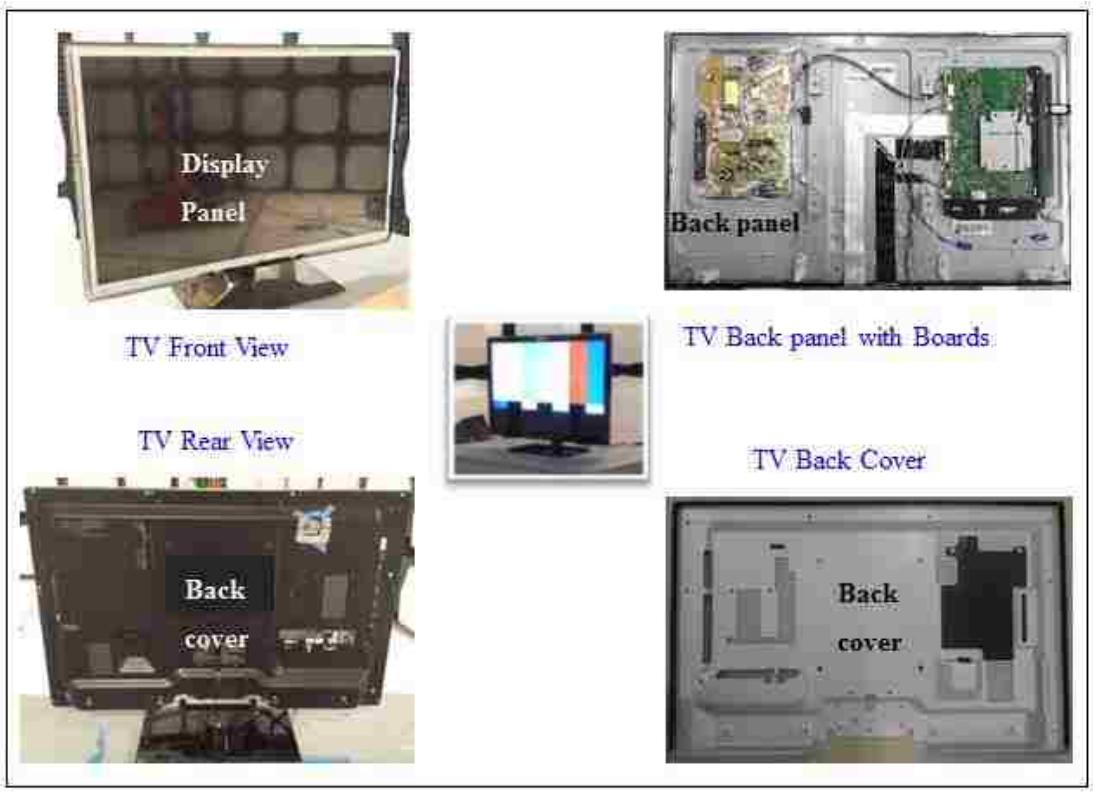

Figure 2.6. Chassis components

2.2. RADIATION PATTERNS

The radiation pattern allows us to determine the direction of maximum radiation for a given frequency. The radiation pattern can be used to identify the probable radiating structures by correlating the radiation pattern to the chassis components. The figures presented below, show the radiation pattern for some of the

peak frequencies. For simplicity, only the data pattern retrieved form the vertical polarization is shown. Figure 2.7 shows the DUT orientation for the radiation pattern. Note that 0 degree is facing the front side of the TV. Figures 2.8, 2.9, 2.10, 2.11, and 2.12 show the radiation patterns for the baseline measurement for the frequencies 138 MHz, 183 MHz, 504 MHz, 540 MHz and 1183 MHz respectively.

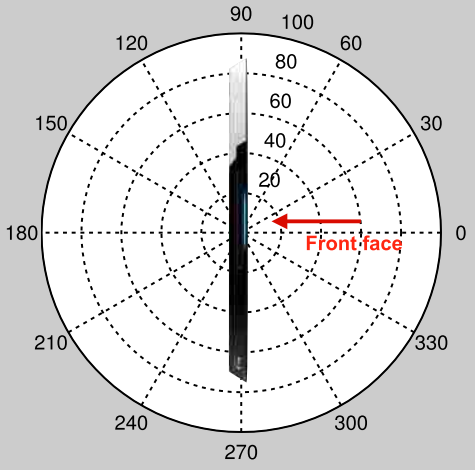

Figure 2.7. DUT Orientation for Radiation Pattern

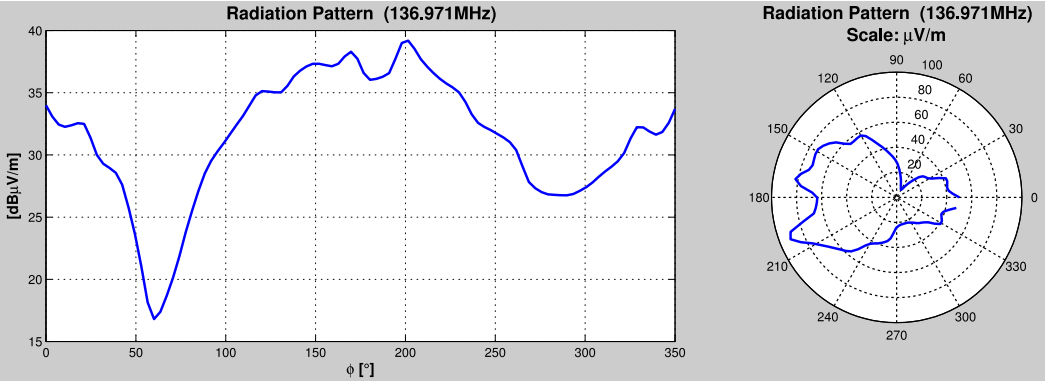

Figure 2.8. Radiation pattern at 138 MHz

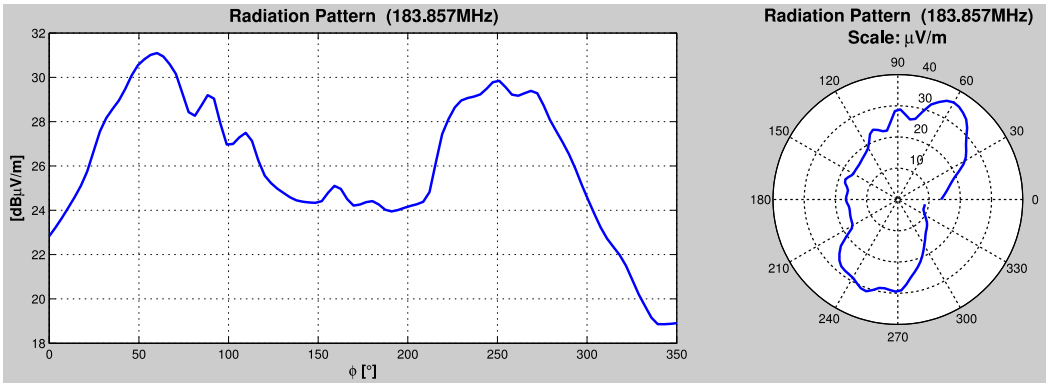

Figure 2.9. Radiation pattern at 183 MHz

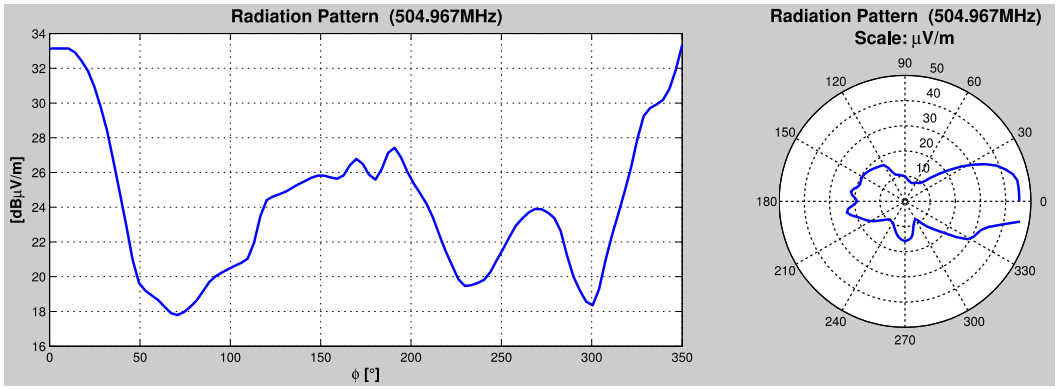

Figure 2.10. Radiation pattern at 504 MHz

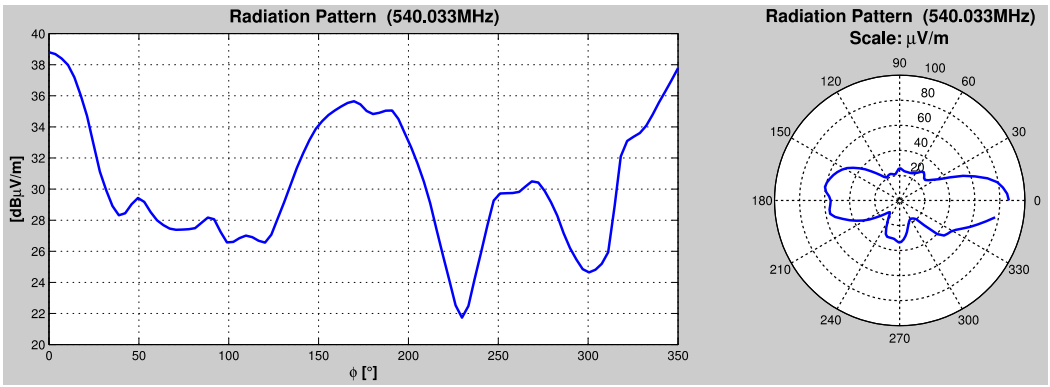

Figure 2.11. Radiation pattern at 540 MHz

Figure 2.13 shows the possible structures that might cause the observed radiation patterns.

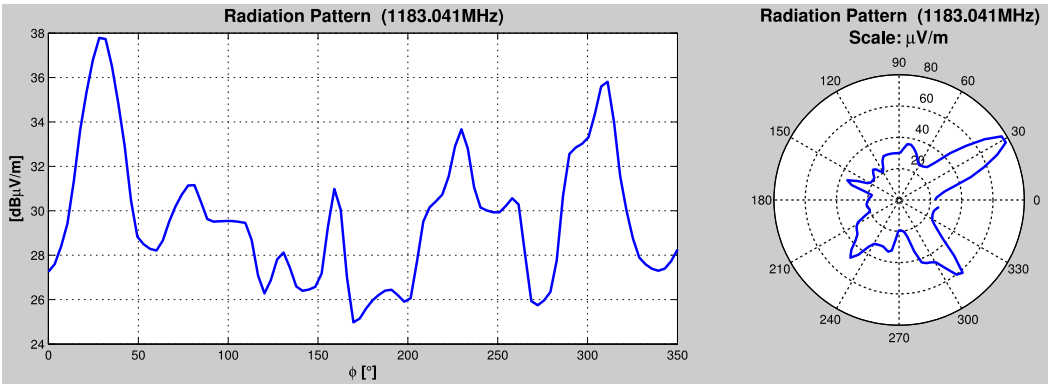

Figure 2.12. Radiation pattern at 1183 MHz

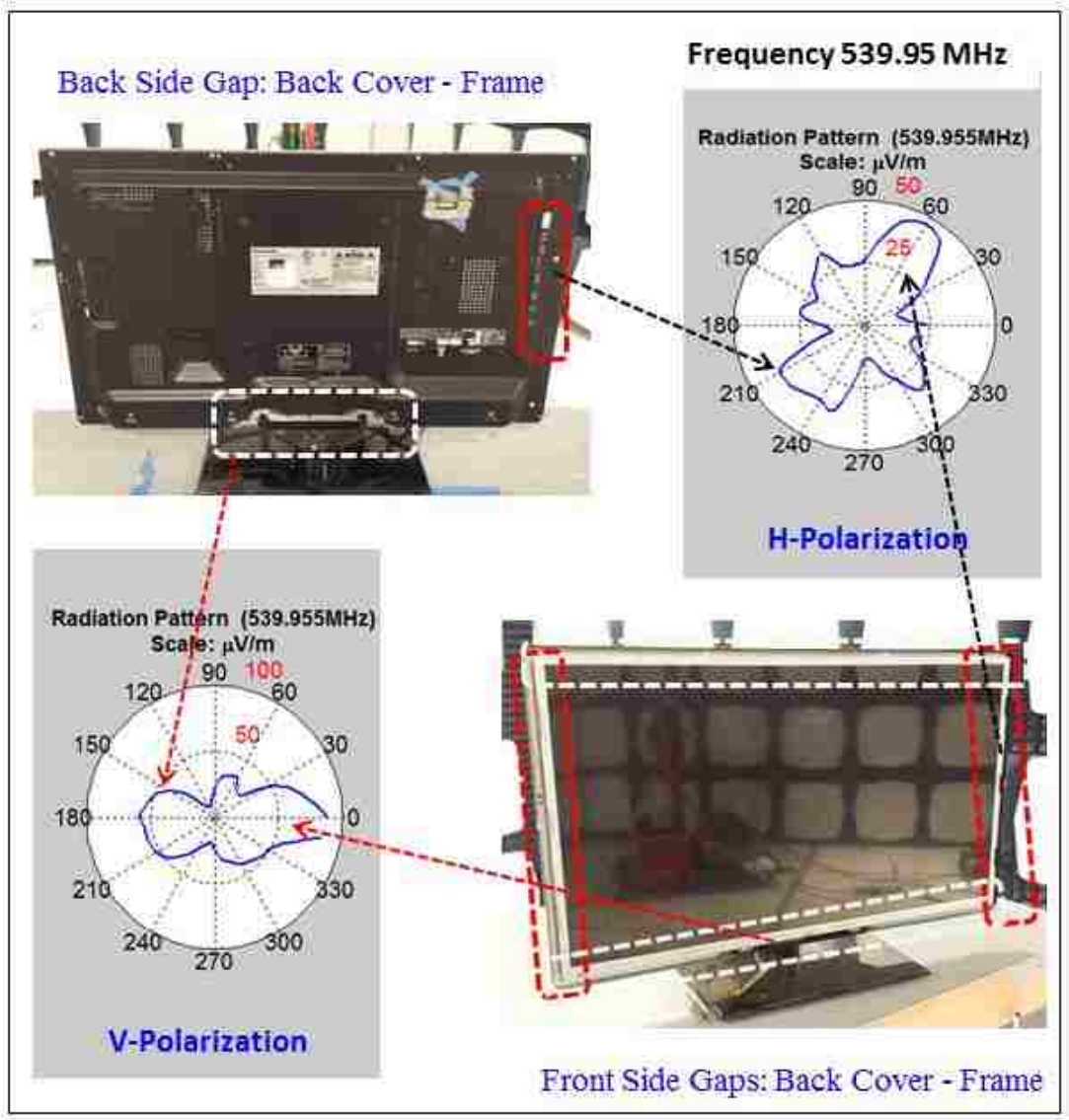

Figure 2.13. Radiation pattern at 540 MHz and possible radiation structures

From the pattern at 540 MHz, it can observed that there is likelihood that the front side radiation in vertical polarization of the antenna is due to front side horizontal gaps, back side radiation in the vertical polarization of the antenna is due to the lower back cover-frame slot and the radiation lobes at 60 and 240 deg. In the horizontal polarization of the antenna are due to the front side vertical gaps.

2.3. RADIATED EMISSIONS FOR SHIELDING MEASUREMENTS

Shielding measurements on the chassis can be performed to identify the radiation sources. From the 'Baseline' radiation pattern and observation of the chassis, we guess that the front and bottom gaps contribute to radiation. To test this, we cover the front gaps with copper tape and re-measure the radiated emissions as shown in Figure 2.14.

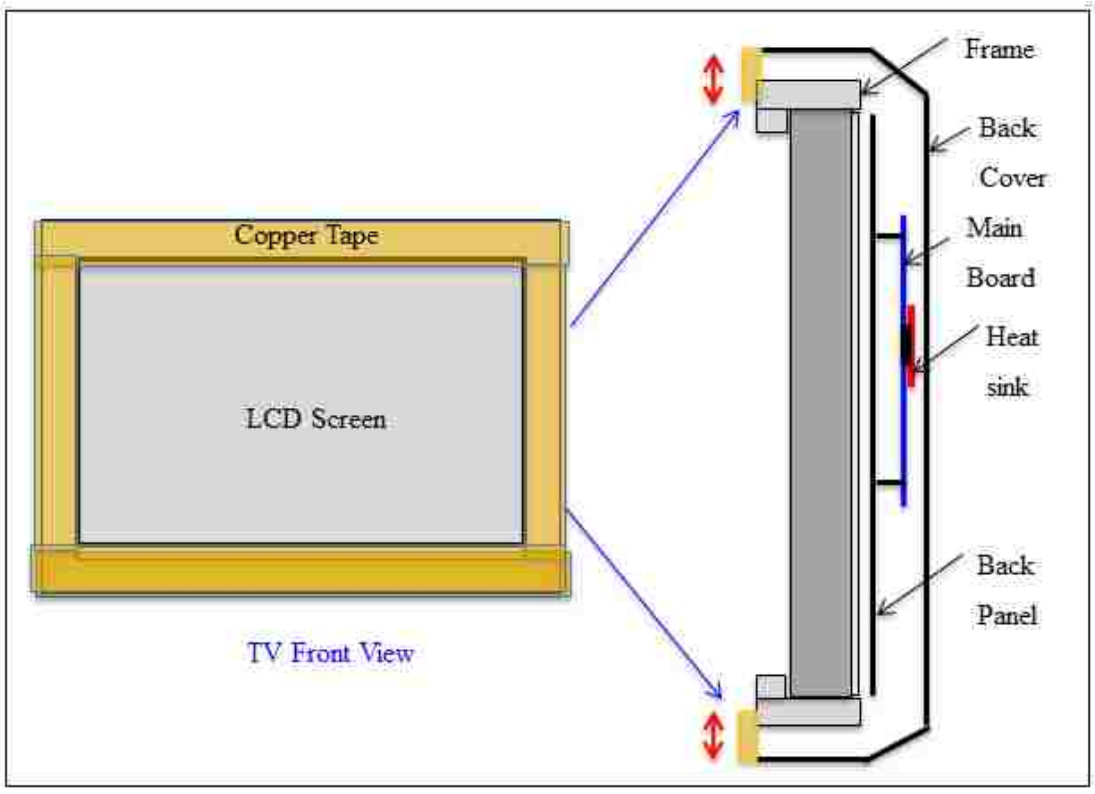

Figure 2.14. Diagram showing the front gaps covered with copper tapper tape

Radiation pattern for the condition where copper tape is used to cover the front gaps indicates that the front gaps contribute to the radiation. Figure 2.15 shows the

photos of the TV in the original condition and with front gaps covered with copper tape and the corresponding radiation patterns for each case.

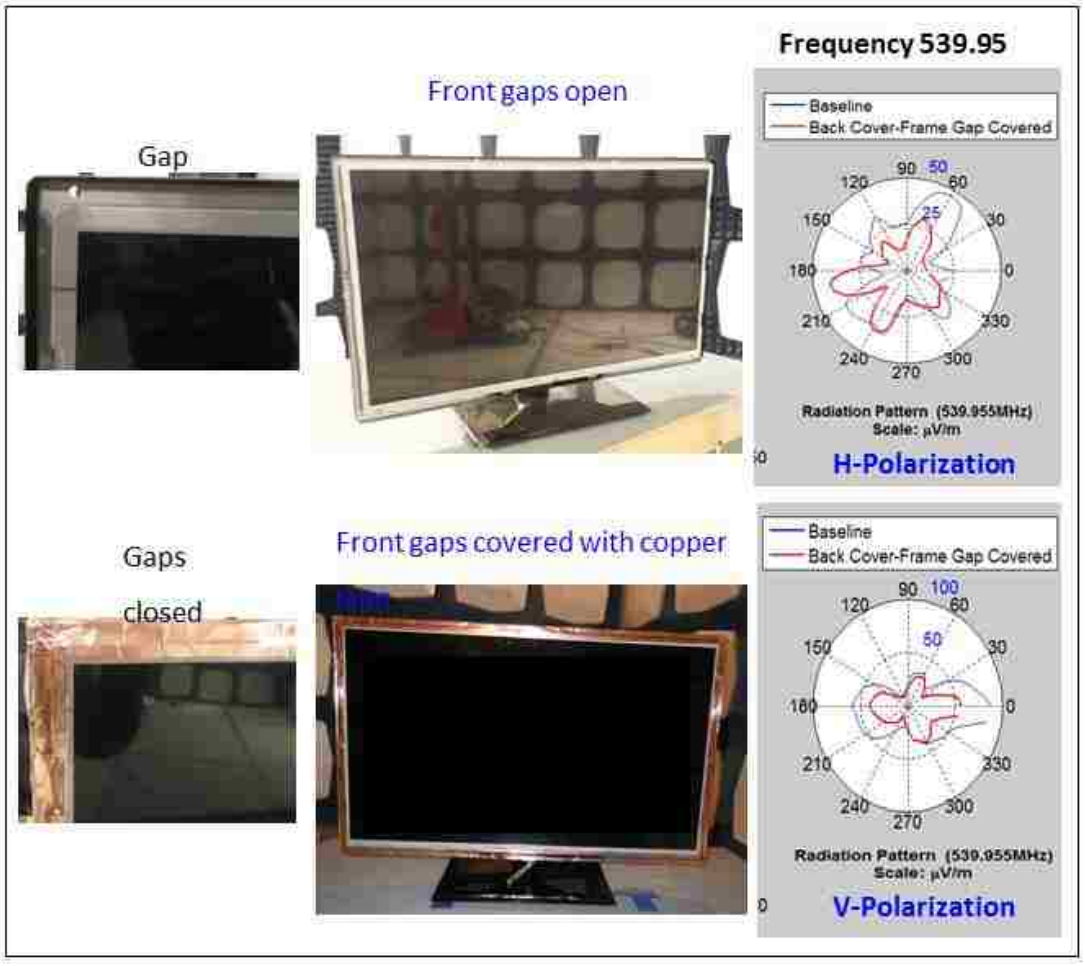

Figure 2.15. Photos of TV with front gaps covered with copper tape and the corresponding radiation pattern at 540 MHz.

The back cover is a large metal piece connected to the back panel with screws. To test if the back cover acts like a shield for the radiations from the main board, we re-measure by removing the back cover from the TV. The radiation patterns measured after removing the back cover are shown in Figure 2.16.

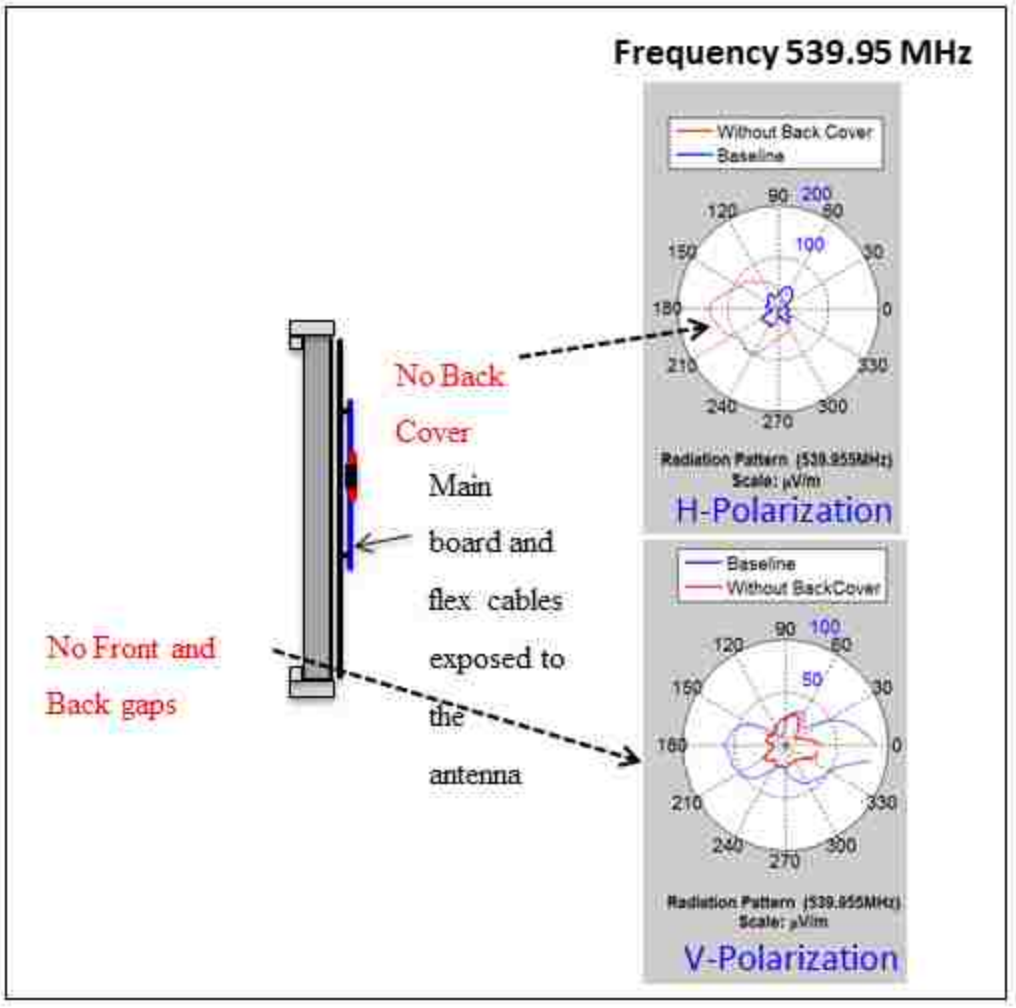

Figure 2.16. Radiation pattern at 540 MHz without the back cover

Front the above measurements without the back cover, we observed that the back side radiations increase in the Horizontal - polarization of antenna due to direct radiation from the main board. Front and Back side radiation reduces in the Vertical – polarization of antenna due to absence of front and bottom gap.

3. TV COMPONENT AND SOURCE IDENTIFICATION

To identify the source of the emission from the TV, we first identify all the electronic circuits and components present within the TV and then perform measurements on them to identify the source.

3.1. IDENTIFYING TV COMPONENTS

Figure 3.1 shows the various electronic components within the flat panel display:

- Main Board
- Display panel
- Display driver board.
- Power board.
- Flex cables.

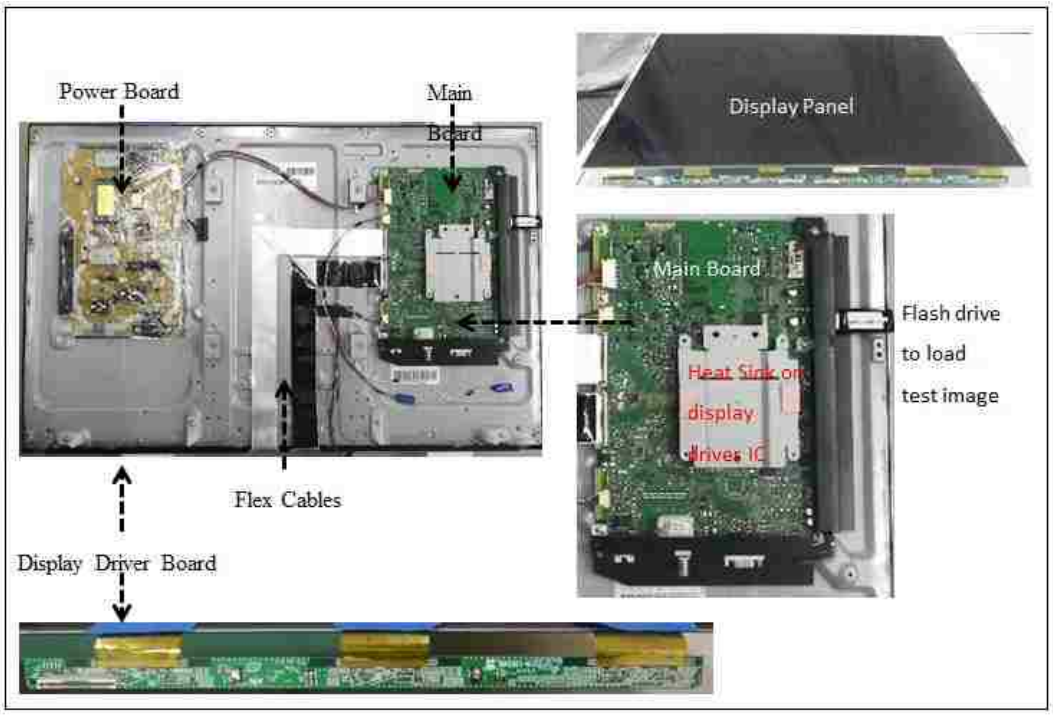

Figure 3.1. Electronic components in the flat panel display

3.2. NEAR-FIELD SCANNING ON THE MAIN BOARD

Manual near-field scanning of internal parts of the flat panel display: A 5mm Hx loop probe was used to probe around the various internal parts of the TV looking for the 506 and 540MHz noise source. Figure 3.2 shows the inside of the TV.

Figure 3.2. Inside of TV1

There are three separate PCB boards connected by various wire and flex cables. The two flex cables were labeled Flex1 and Flex2. In the previous investigation we used a current clamp on all the wire cables to observe the current, and none of them showed the noise of our interest. Figure 3.3 shows the close-up around the flex cables and A-board.

The flex cables are routed in such ways that the signal traces are facing towards the front panel. The side facing towards the black panel seems to be solid return plane. Probing around these solid return plane regions didn't show anything. There were some regions where the flex cables are folded over that the signal traces were exposed. Figure 3.4 shows the area where the near-field was measured. The near-field was measured using a 5mm Hx probe and a 15dB pre-amp. The spectrum

analyzer was set to max hold while the probe was moved around these exposed regions.

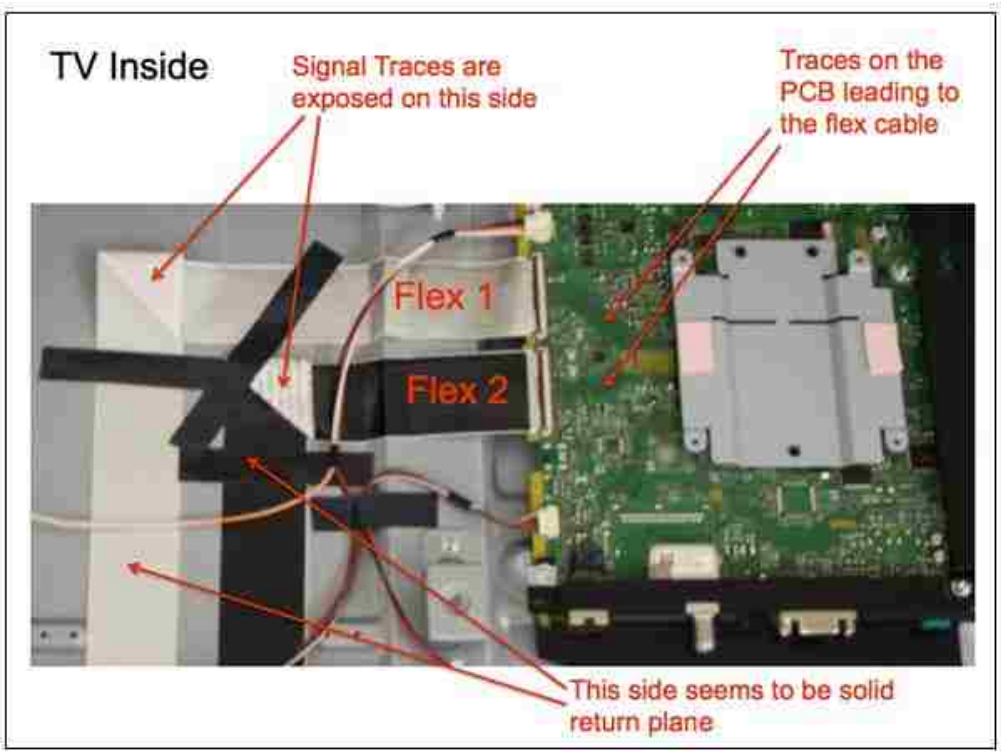

Figure 3.3. Close-up of Flex Cables and A-board

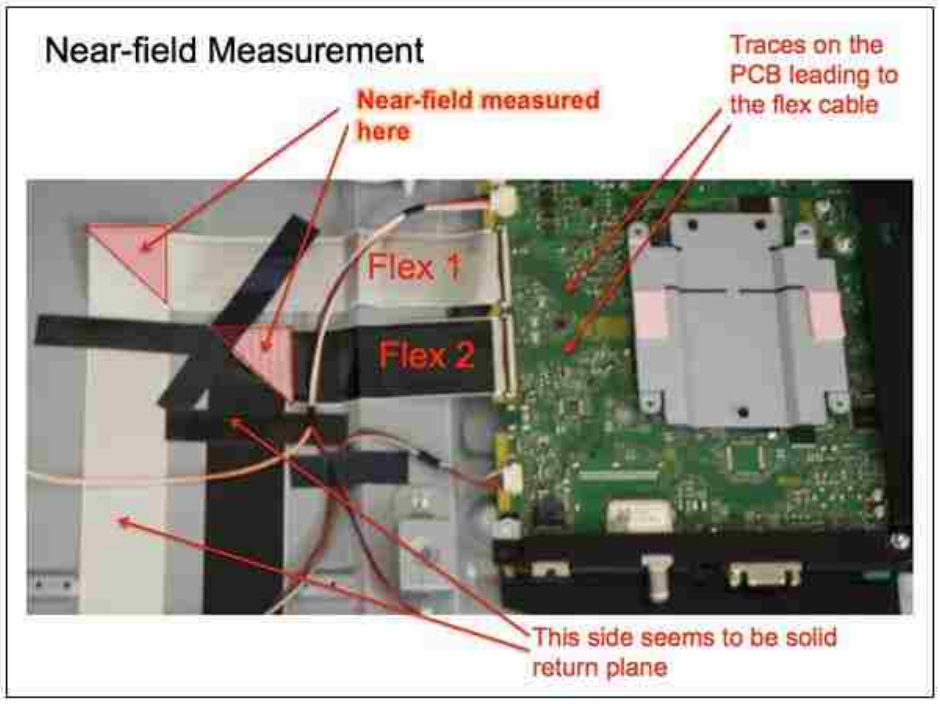

Figure 3.4. Areas of Exposed Traces on Flex Cables

Figure 3.5 shows the measured near-field around the exposed regions of the flex cables.

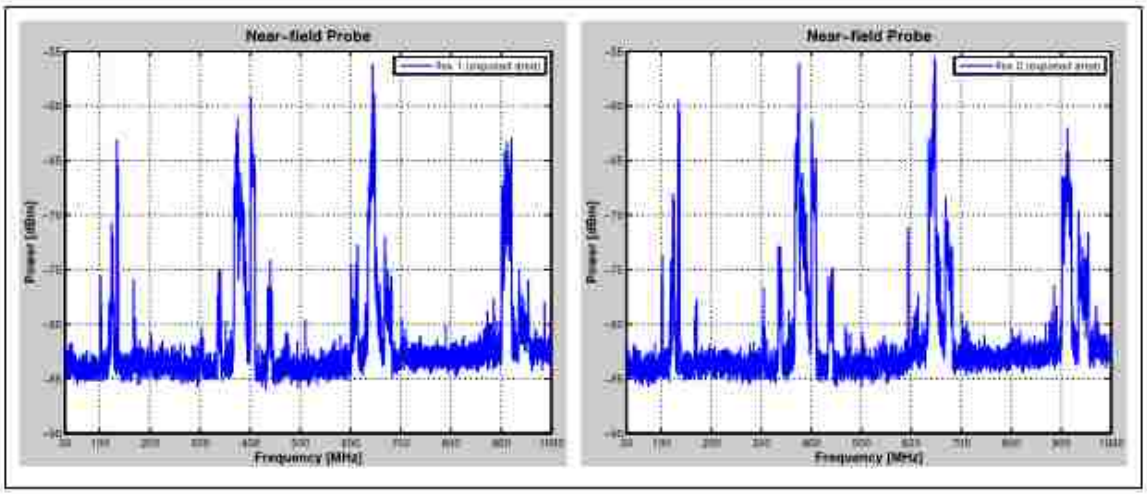

Figure 3.5. Near-field Around Exposed Regions of Flex Cables

There is significant noise at a few different frequencies, but 506, and 540MHz were not visible. The reason for this could be because we were only measuring a small portion of the cable. Next, the near-field was measured around different area on the A-board. It was observed that around the traces that comes from the main processor IC to the flex cable connectors contained the noise at 500 and 506MHz. Figure 3.6 shows the locations of near-field measurement. Again, the probe was moved around each regions and max hold was used.

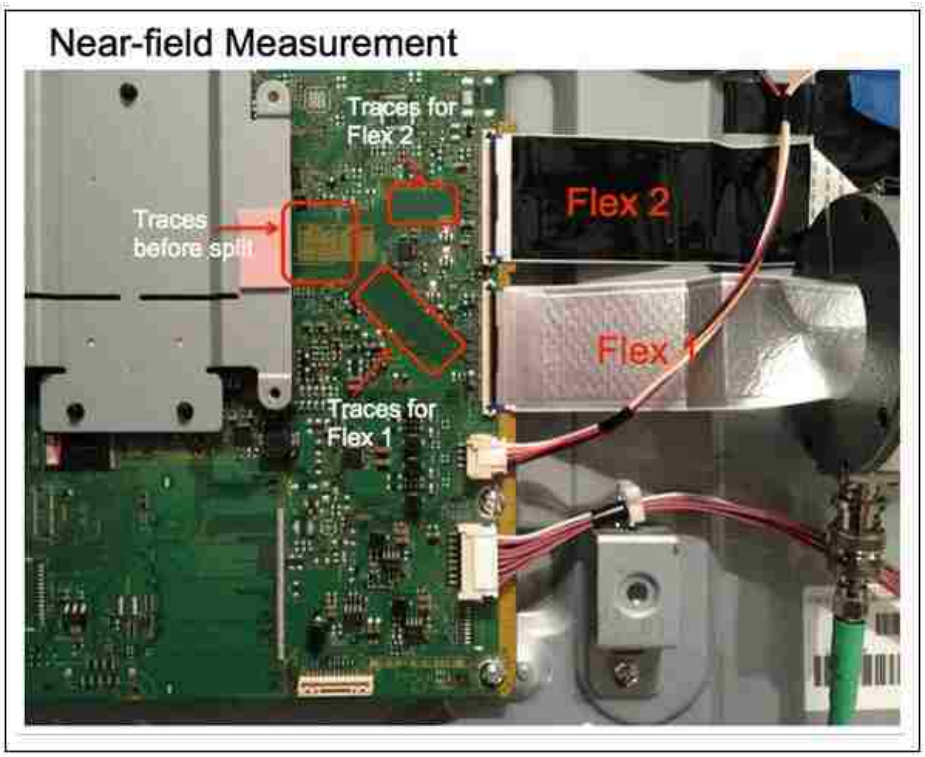

Figure 3.6. Near-field Probing around A-board

In 3.7, the near-field around the traces before splitting into two branches shows both 506 and 540MHz noise. After the traces split into two branching leading to flex1 and flex2, only 540MHz noise was visible.

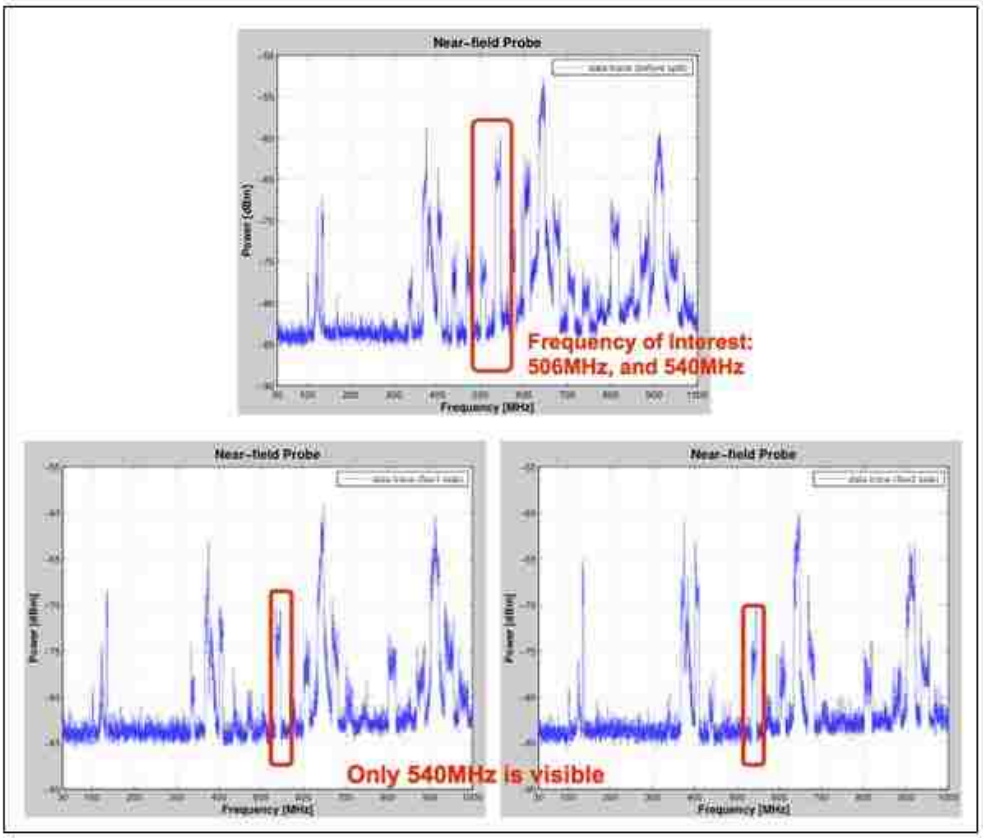

Figure 3.7. Measured Near-field data around A-board

It is possible that the 500MHz got weaker in those regions and our measurement was not sensitive enough to pick up. Later we used Hz probe to scan while the probe was landing on the surface of the PCB, and 500MHz was still visible in these region.

Common-mode Current Measurement on Flex Cables a F-65 current clamp was used to measure common-mode current on the flex cables as shown in Figure 3.8. Figure 3.9 shows the measured common mode current on Flex 2.

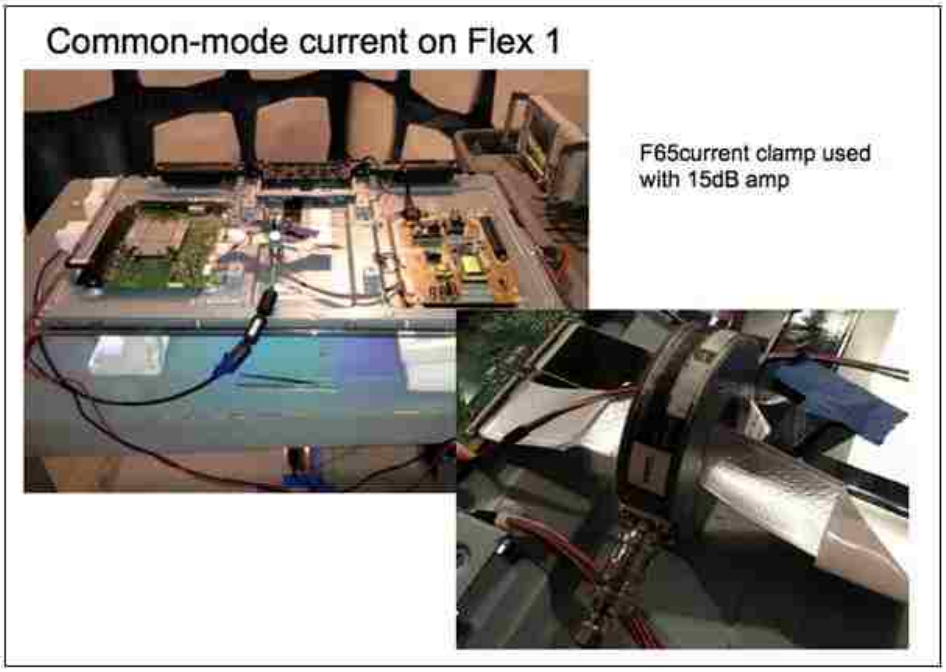

Figure 3.8. Common-mode Current Measurement on Flex1

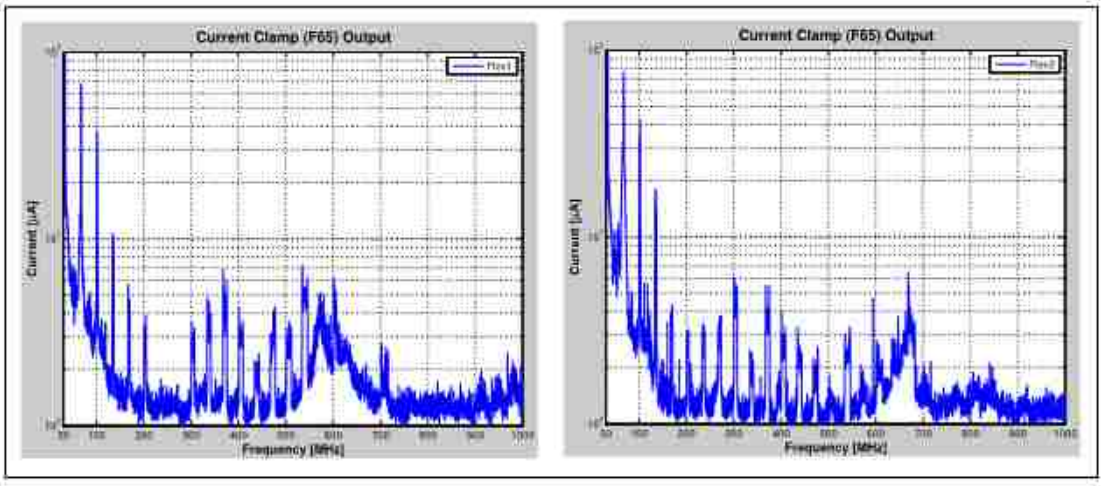

Figure 3.9. Common-mode current on Flex 2

The current clamp output for both flex cables show 540MHz. 506MHz is shown in Flex1 but not in Flex2. The zero span at 506 and 540 MHz was observed and showed similar 60Hz and 66KHz modulation observed in radiated emissions. Next, a ferrite clamp was placed on the flex cable and the change in common-mode current was observed. The model number for the ferrite clamp was Laird 28S2001-2A2.

Figure 3.10 shows the ferrite characteristic curve from the datasheet. Note that our ferrite is made of material 28, which is supposed to be most effective at 4-500MHz range.

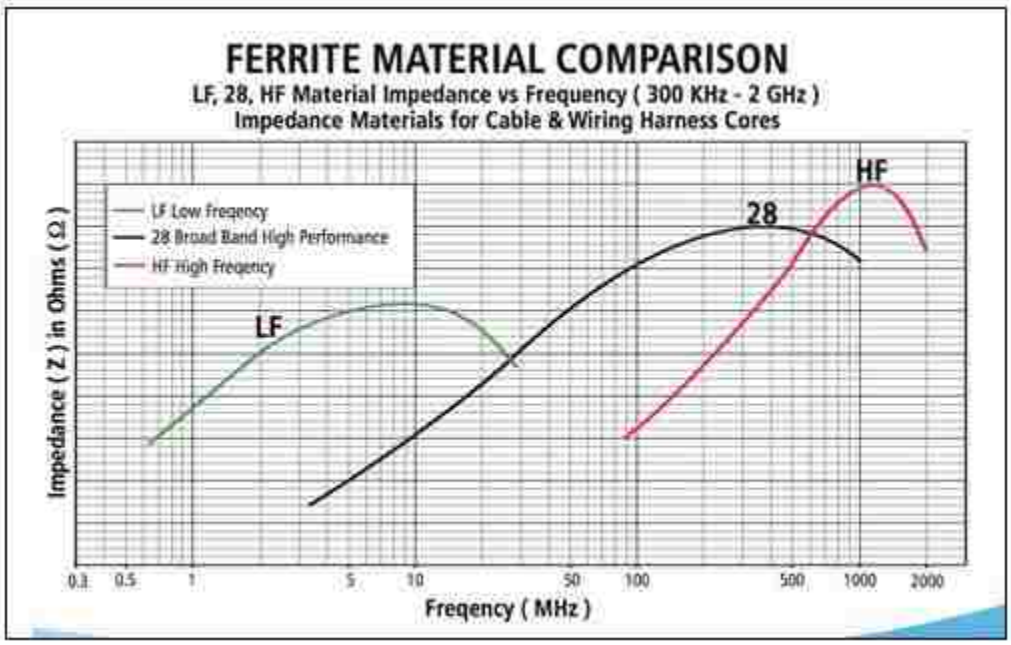

Figure 3.10. Ferrite Clamp Characteristic Curve

Figure 3.11 shows the comparison of the current clamp output with and without ferrite.

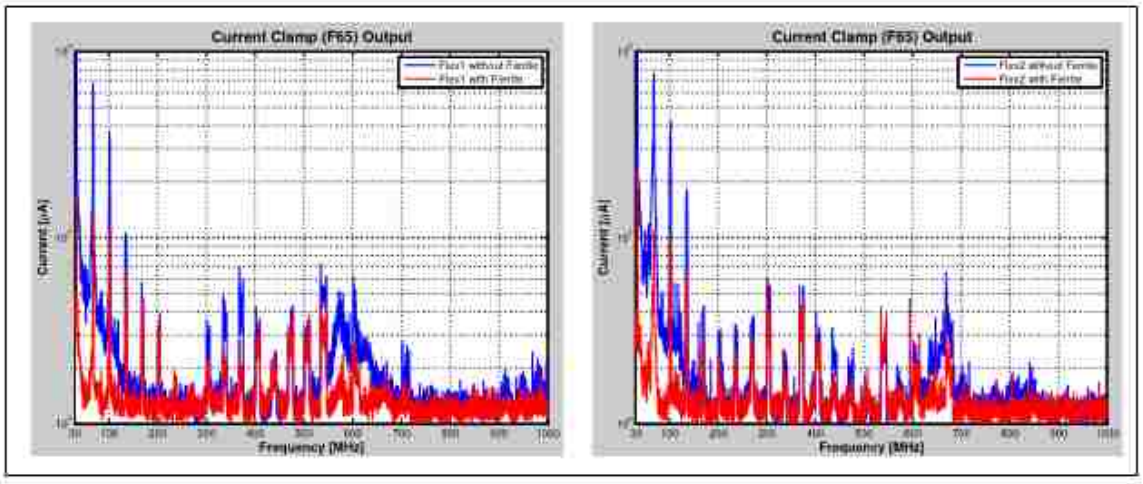

Figure 3.11. Effect of Ferrite Clamp

The ferrite clamp reduced current at some frequencies. However, it doesn't seem to be so effective at 500MHz range. The reason for this could be because the ferrite impedance is still not enough with respect to the source impedance and common-mode impedance of the cable. This test was just done to observe the effect of ferrite we had in our hand. The measurement results clearly show that the 506 and 540MHz noise is visible in the traces connecting the main IC to the flex cable connectors, and on the flex cables.

Near-field probing around Flex Cable: A 5mm Hx probe was used to probe over the reference plane side of the two flex cables. Spectrum analyzer was set to max hold while the probe was moved around the region marked in the Figure 3.12.

Figure 3.12. Probed Area of the Flex Cable

Figure 3.13 shows noise at 506 and 504MHz. This is consistent with current clamp measurement where we observed the same spectrum in the common-mode current.

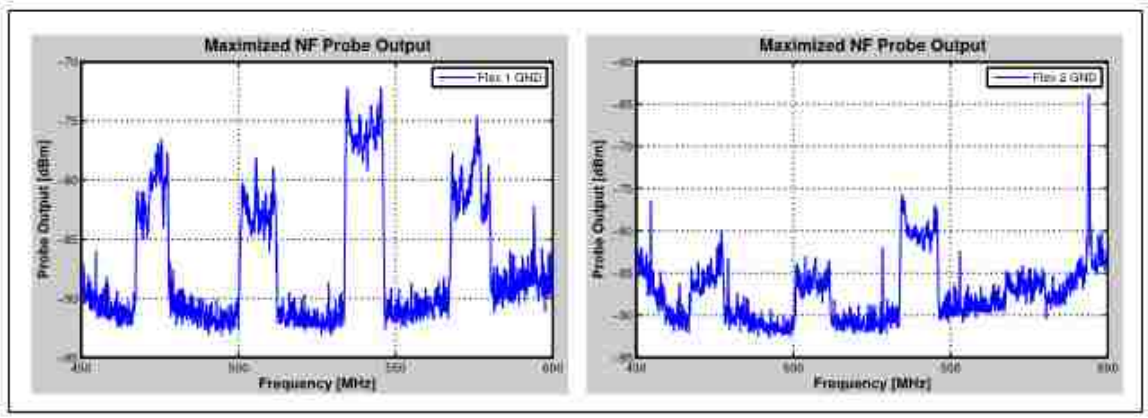

Figure 3.13. Maximized Probe Output over Flex 1 and Flex 2

Next, an area of the back panel near the flex cable was probed to see if there is any surface current on the back panel. The Figure 3.14 shows the probed area.

Figure 3.14. Probed Area on Back Panel

The cable bundle that crosses the area was moved aside during measurement and the Hx probe was moved around the back panel while placed against the panel.

Figure 3.15 shows that 540MHz noise is definitely visible on the back panel indicating that the noise current is flowing on the surface. 506MHz noise was not

visible in this result, and the possible reason could be because the signal was too low and masked by other broadband noise.

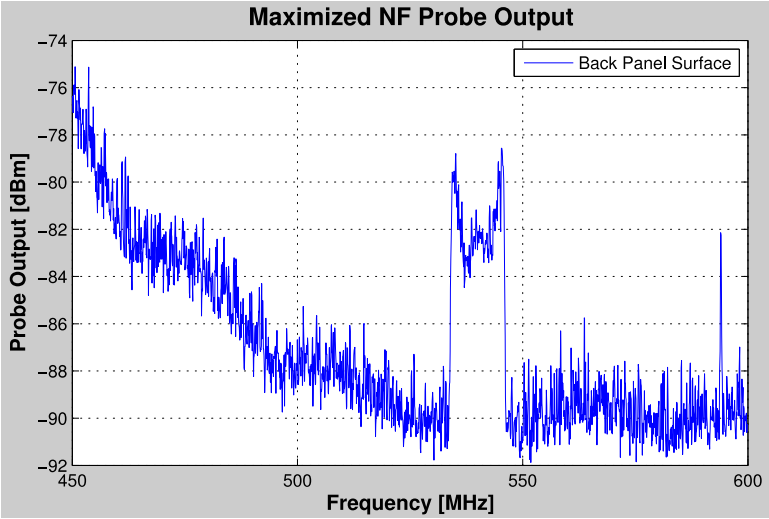

Figure 3.15. Maximized Probe Output over Back Panel

Automated Near-field Scan: Automated near-field scan was performed to observe the field distribution around the A-board and flex connectors. A 6mm Hz probe was used with a 15dB pre-amp. Frequency range was from 30MHz – 2GHz. Figure 3.16 shows the scanning area. 5mm step in both x and y direction was used. The probe was set to land on all points to capture the maximum signal. Note that the heat-sink on the main IC was removed so the fields around the IC can be also scanned.

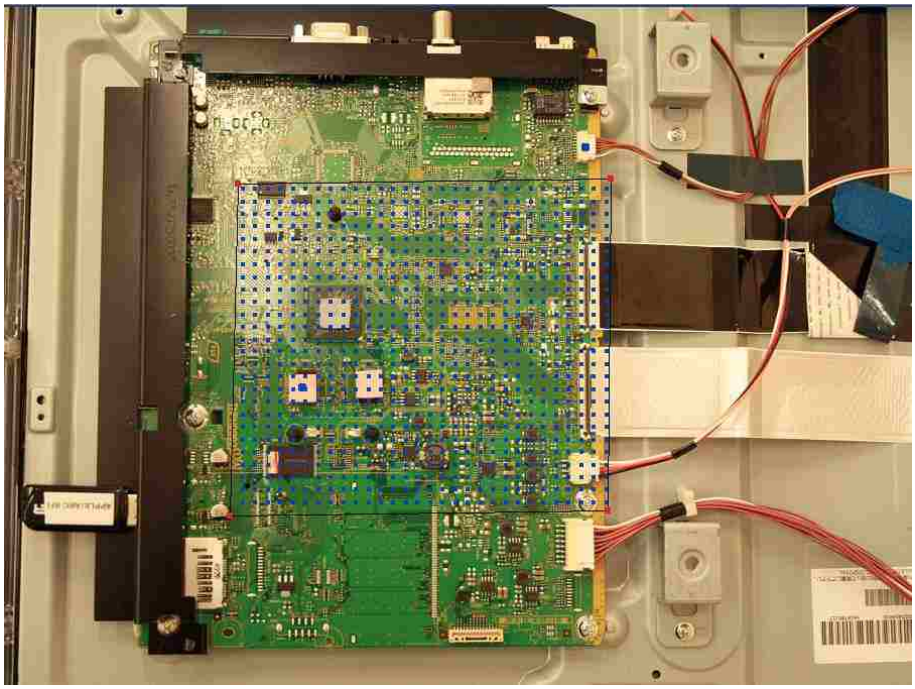

Figure 3.16. Automated Near-field Scanning Area

Clearly, the data traces coming from the main IC has 506 and 540MHz noise in the spectrum. Figure 3.17 and Figure 3.18 show the field distribution of 506 and 540MHz noise respectively.

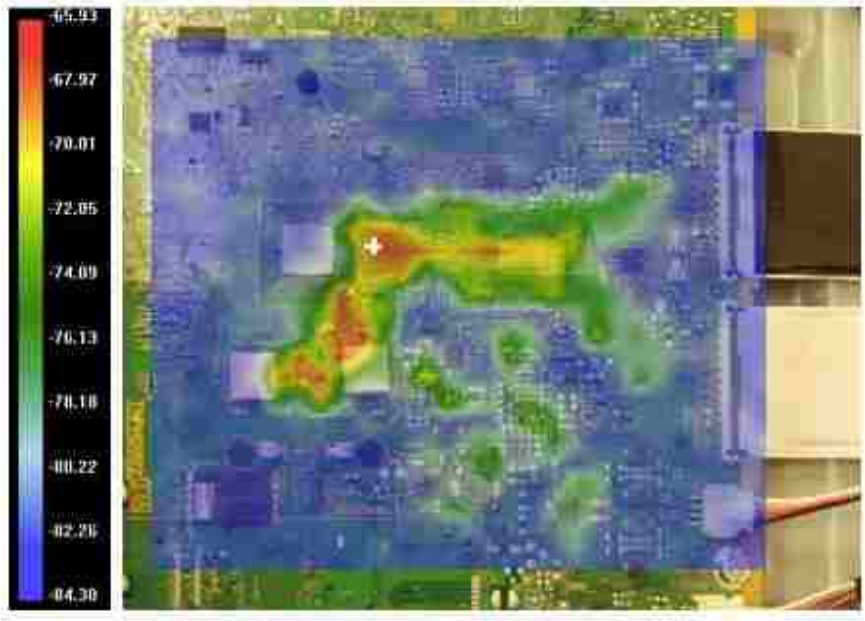

Figure 3.17. Field Distribution for 506MHz

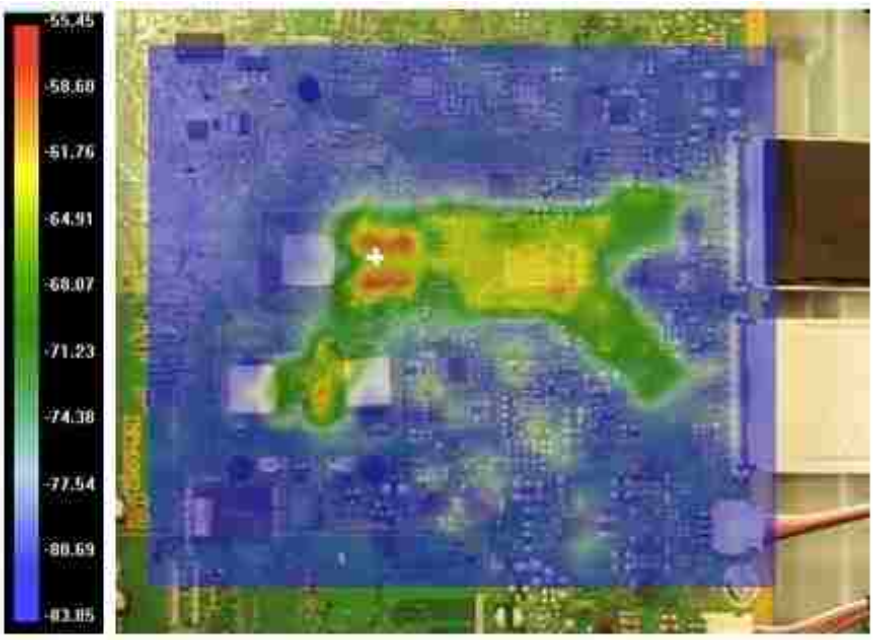

Figure 3.18. Field Distribution for 540MHz

It can be seen from Figure 3.17 and Figure 3.18 that the 506 and 540MHz noise is mostly concentrated around the data traces coming from the IC to the flex connector. It was observed that field distribution for the most of the data signal spectrum in Figure 3.19 is distributed similarly as shown in Figure 3.18 (for 1077MHz).

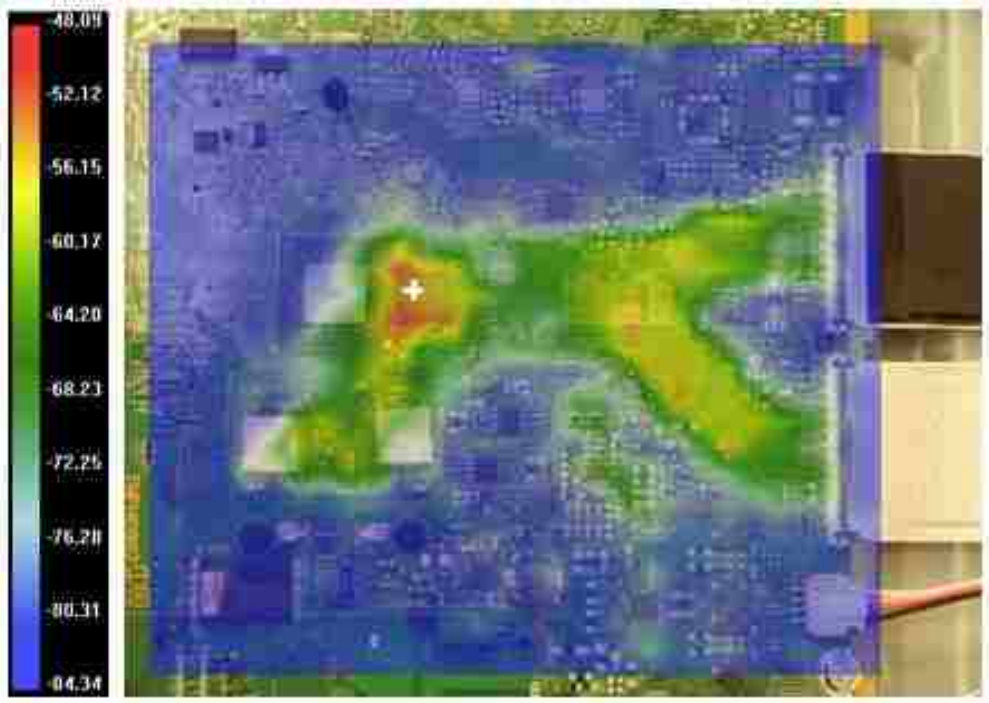

Figure 3.19. Field Distribution for 1077MHz

3.3. DIRECT PROBING ON THE MAIN BOARD

To observe the time domain characteristics of the LVDS clock signal, we directly probe on the main board. The flex cables are removed from the main board and the LVDS traces are terminated with 0402 too-ohm LVDS termination. The probing is carried out using 1.1-k-ohm resistors in series with two equal length semi-rigid cables. An oscilloscope is used to measure the signals.

The measurement setup for the direct probing is described in Figure 3.20.

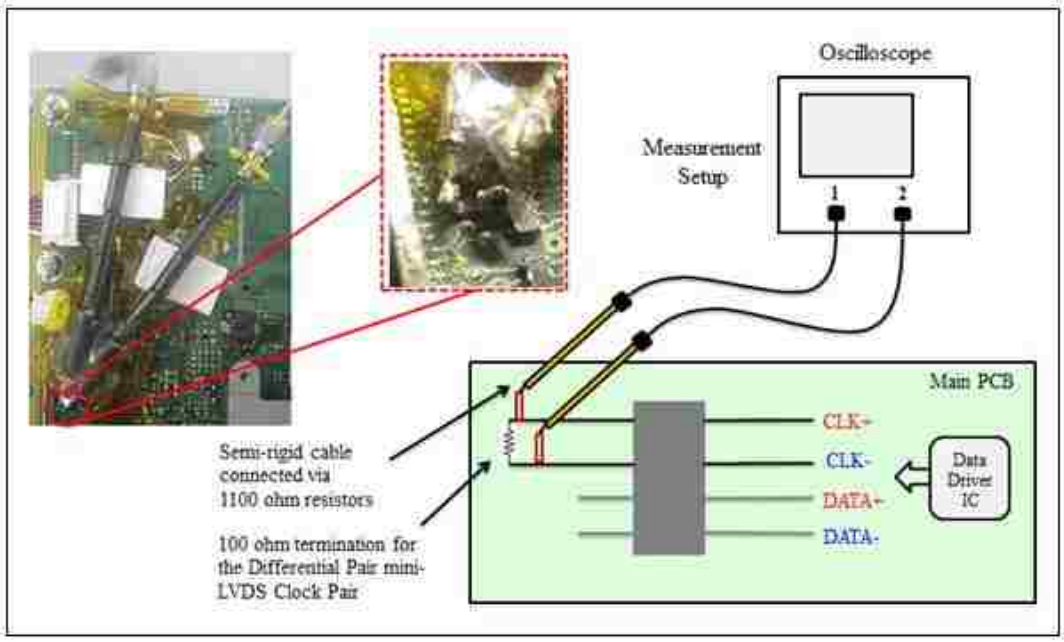

Figure 3.20. Direct probing on the main board after removing the flex cables.

3.4. MINI-LVDS CLOCK SIGNAL

The Figure 3.21 shows the measured clock signal. The frequency of the clock signal as measured is 133 MHz.

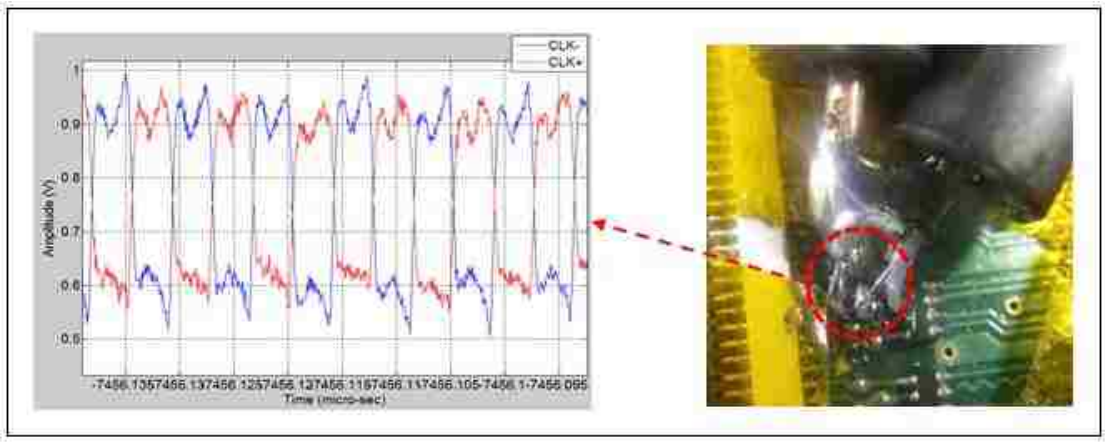

Figure 3.21. Measured waveform of the 133 MHz mini-LVDS clock signal.

The Figure 3.22 shows the measured clock signal and the difference in the amplitudes of the two differential channels.

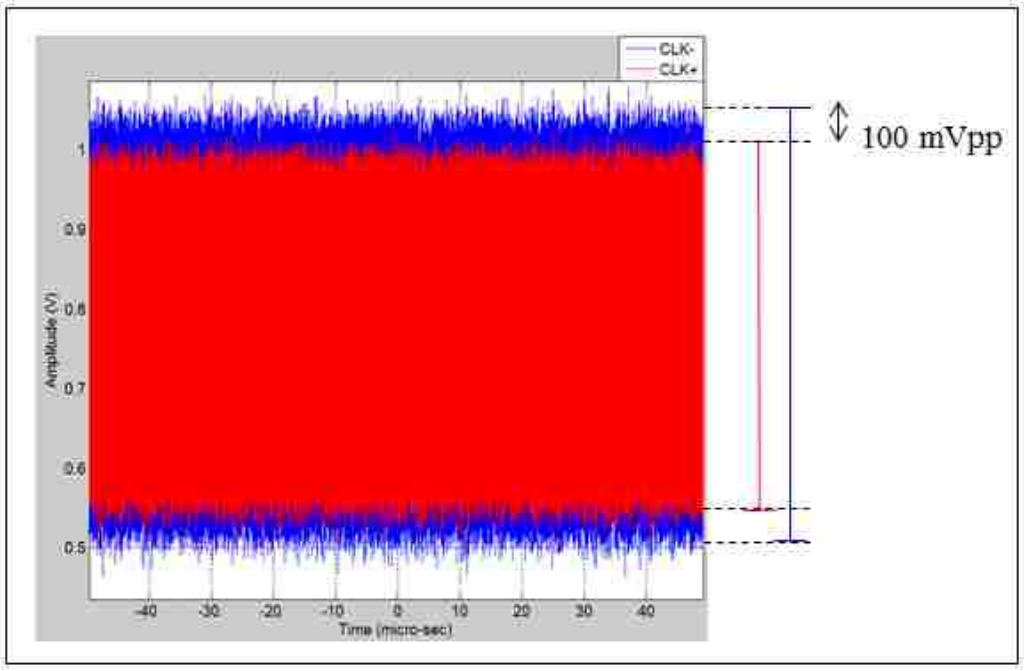

Figure 3.22. Plot of the measured differential signal showing amplitude asymmetry.

The amplitude asymmetry in the LVDS clock signal can drive a common mode noise voltage with the main board ground as reference. The can be one possible mechanism for the presence of a common mode source.

Figure 3.23 shows the calculated common mode and differential mode spectrums for the measured time domain clock mini-LVDS clock signal – which shows the presence of the 506 MHz and 540 MHz in the common mode spectrums.

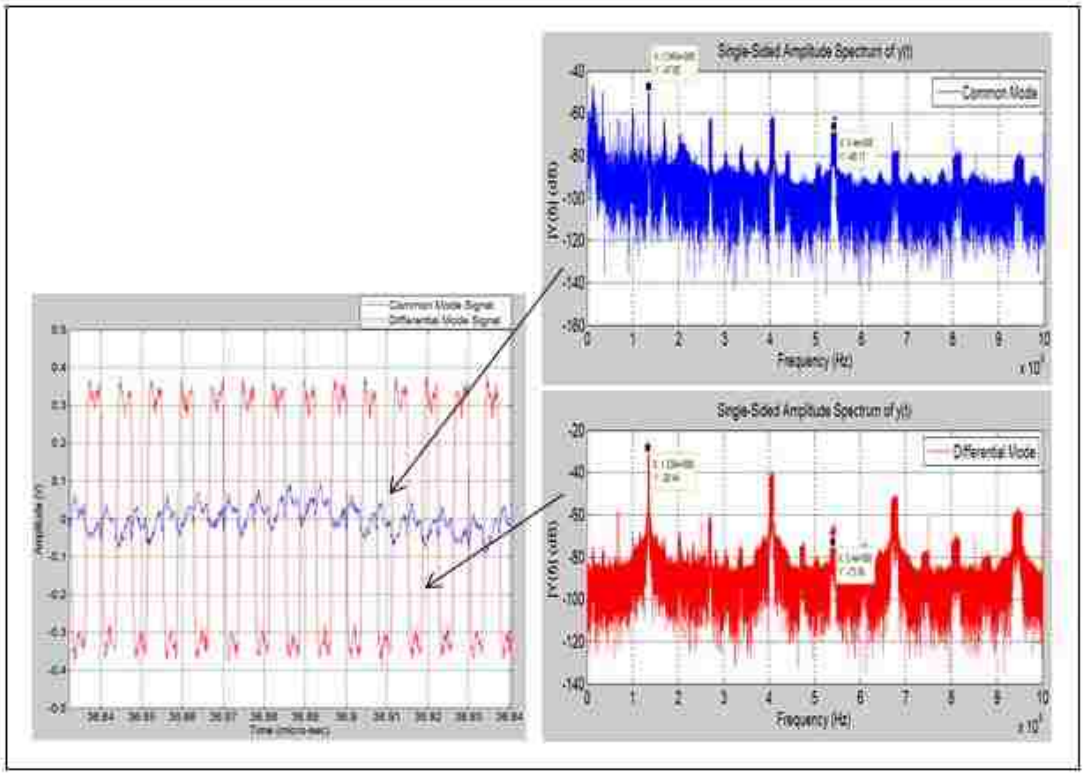

Figure 3.23. The calculated differential mode and common spectrum of the measured time domain mini-LVDS clock signal.

4. INDIVIDUAL COMPONENT MODELING

4.1. MODELING APPROACH AND METHODOLOGY:

The complete TV model is built up by first individually modeling the various components using the full wave modeling tool – CST MWS. The main components modelled are the chassis, main board, flex cables, and the LCD driver board. The CAD models of the chassis are imported directly into CST. Excitation ports and mesh settings are applied to the model and the model simulated. The model is validated by comparing the simulation results with the measurement results.

The full wave models for the individual components have been validated and can be combined to form the complete model of the TV. The simulated results for the full model are validated with measurements. The full wave models can be used to predict the far-field radiations from the TV under different geometric conditions of the components. Using the field monitors at specified frequencies, radiation mechanisms can also be analyzed.

For the prediction of the radiated emissions from the TV models, we first use the common mode model of the TV, which consists of the common mode models of the flex cable, and the LCD driver board. These models are a simplification and consist of only the shield/return parts of the flex cable and the LCD driver board. Since the signal and ground traces of the components are not modelled, the overall mesh size is relatively small and the results are available for comparison relative much faster. Thus, first we validate the common mode model of the TV chassis step-by-step by adding each component and comparing with measurements. Using field monitors in the common mode models, we can analyze the excitation and radiation mechanisms. This approach becomes the basis for the analysis of the complete model.

The full-wave modeling approach is as described in Figure 4.1 -

- Full-wave models of individual components are created and validated with measurements.
- Full wave modeling tool: CST Microwave (Time Domain Solver).
- Individual components combined to form the complete model.

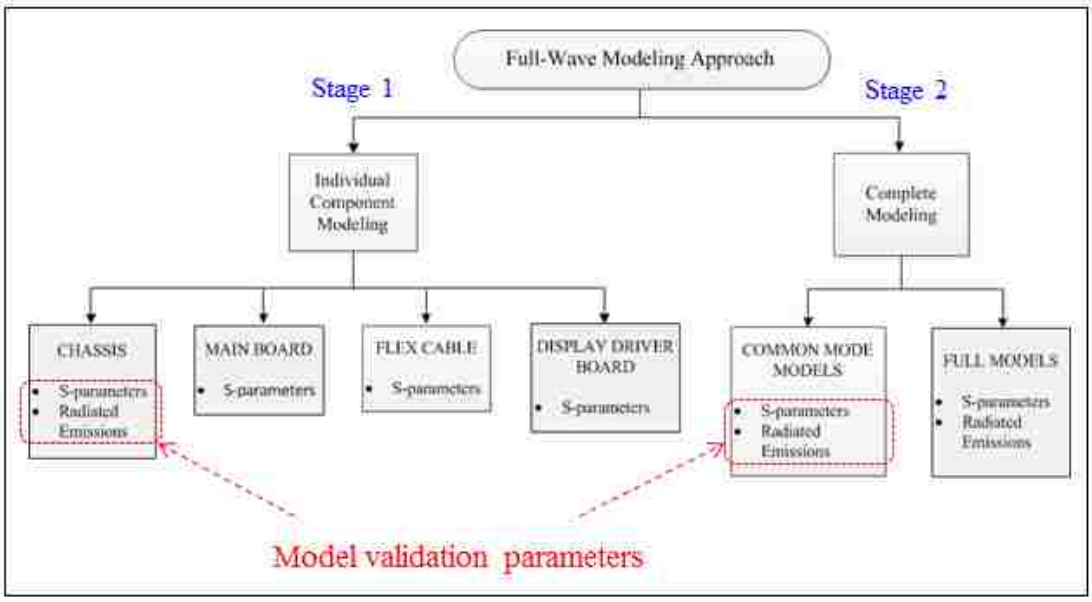

Figure 4.1. Full-wave modeling approach

4.2. CHASSIS MODELING:

The chassis consists of the following four components:

- Back Panel (Metallic)
- Back Cover (Metallic)
- Frame (Metallic)
- Dielectric spacer between frame and back panel. (a type of plastic material)
- Metallic Screws – **11** (connecting frame and back panel) and **9** (connecting back panel and back cover)

The chassis simulation model setup is validated by using two parameters:

- S-parameters.
- Radiated emissions.

4.2.1. Modeling Challenges. One of the significant modeling challenges pertains to the repeatability in measurement. This is due to the multiple points where the chassis parts loosely connect to one another and the large number of screws that connects different parts. It is important to make sure that the measurement conditions are exactly similar to the contact conditions in the simulation model.

4.2.2. Methods to Overcome Challenges. To make the chassis condition exactly similar to the simulation model, the following steps were taken - gaskets wear added to certain areas, which had loose-contact, shown in Figure 4.2.

Figure 4.2. Gaskets connections on back panel for better contact to back cover

Mylar tape was used as insulation where there were unintended contacts, as shown in Figure 4.3.

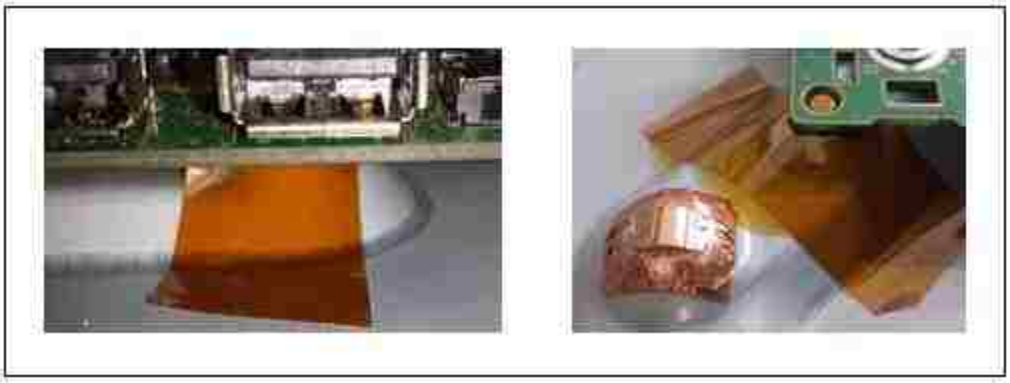

Figure 4.3. Mylar tape under the main board to prevent contact of back panel to the main board

4.2.3. Part 1 of Validation of Chassis Model Using S-parameters. For modeling the back panel and the frame, two ports are connected between the back panel and frame on the back side of the flat panel display and the s-parameters are measured. The same port locations are kept for the simulation models and the results are calculated and compared with the measured s-parameters to validate the simulation model.

The components modeled are shown in Figure 4.4.

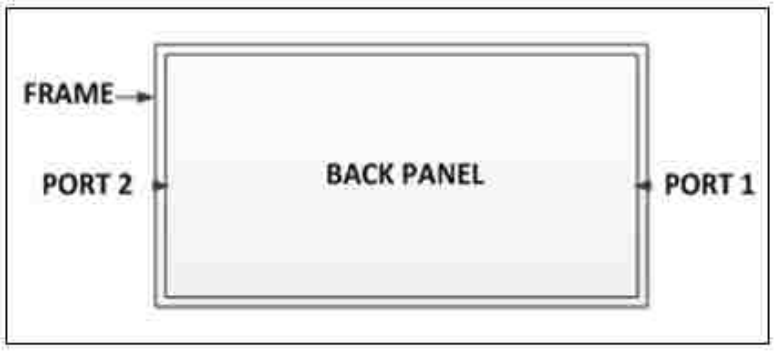

Figure 4.4. Components modeled

Figure 4.5 shows the simulation model.

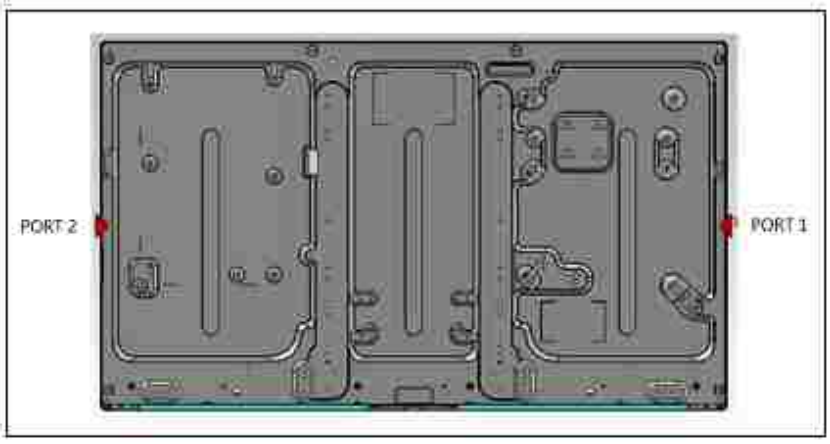

Figure 4.5. Simulation Model

Figure 4.6 shows the measured chassis with the port location.

Figure 4.6. Measured chassis

Figure 4.7 shows the simulation and measurement comparison.

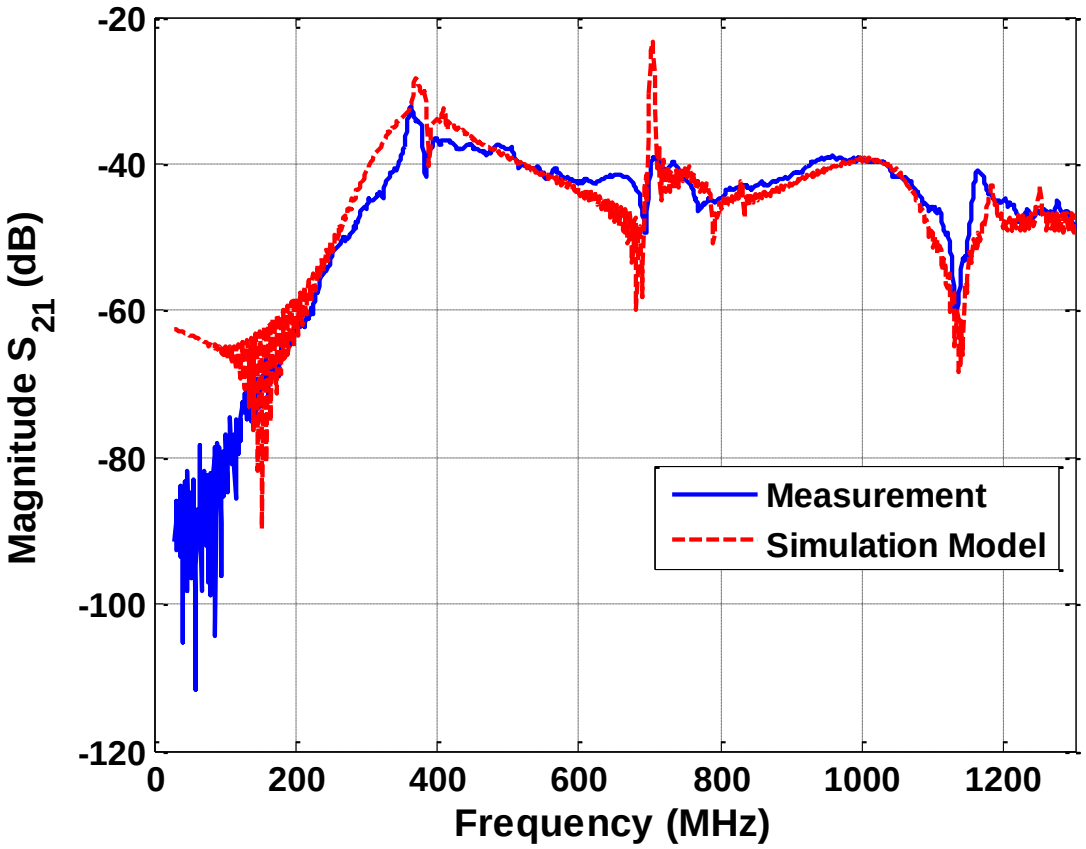

Figure 4.7. Simulation Vs Measurement

As can be observed from the result comparison in Figure 4.7, a relatively good matching is obtained between the simulation and the measurement result. The higher Q-factors of the resonances of the model can be corrected by addition of lossy material to the model.

4.2.4. Part 2 of Validation of Chassis Model Using S-parameters. Ports placed across the back cover – frame gaps.

The components modeled are shown in Figure 4.8.

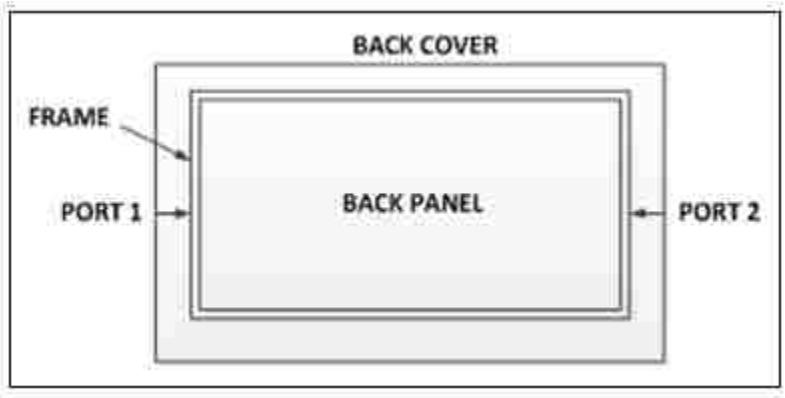

Figure 4.8. Components modeled

Figure 4.9 shows the simulation model.

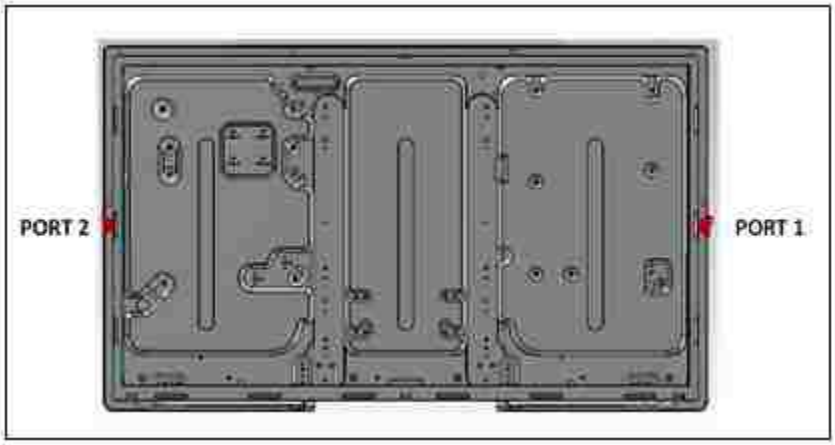

Figure 4.9. Simulation model

Figure 4.10 shows the measured chassis with the port location.

Figure 4.10. Measured chassis

Figure 4.11 shows the simulation and measurement comparison.

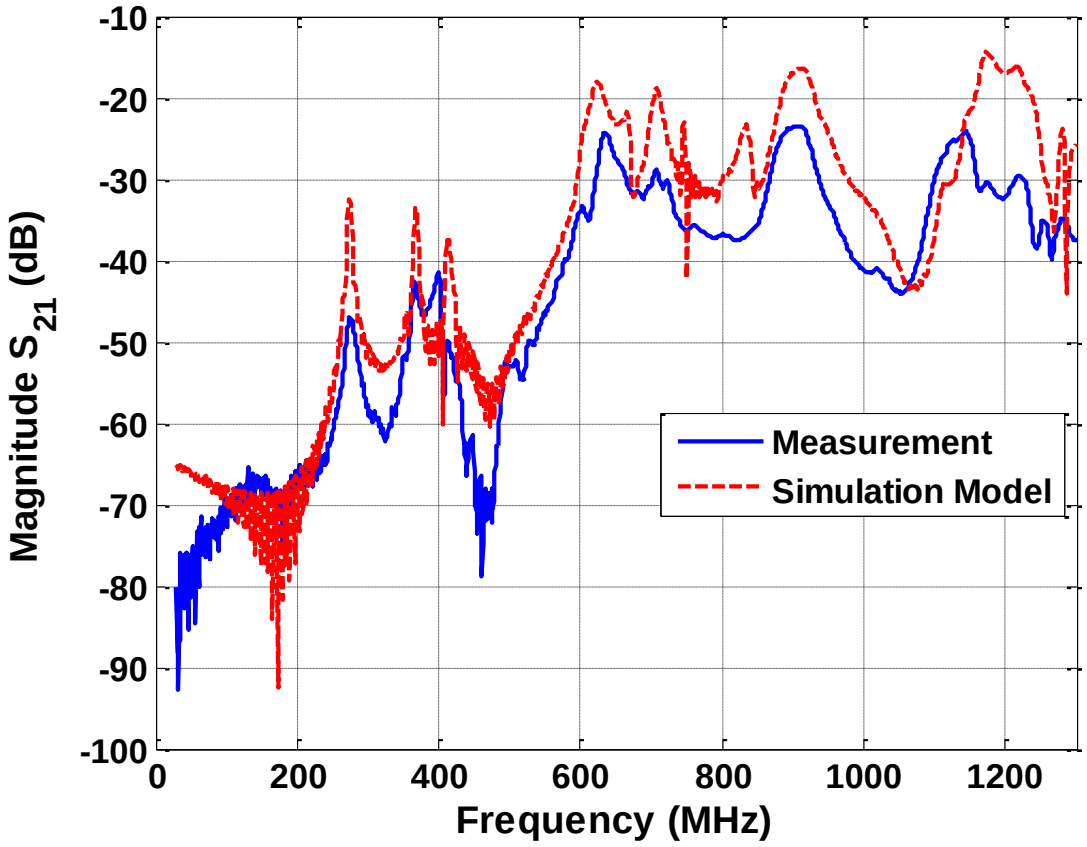

Figure 4.11. Simulation Vs Measurement

As can be observed from the result comparison above, a relatively good matching is obtained between the simulation and the measurement result. The higher Q-factors of the resonances of the model can be corrected by addition of lossy material to the model.

4.2.5. Part 3 of Validation of Chassis Model Using S-parameters.

Validation of the coupling within the chassis model is done by exciting the back panel with a small (3cm x 3cm) metal patch and measuring the gap voltage in the front gaps (between the back cover and the frame).

The components modeled are shown in Figure 4.12.

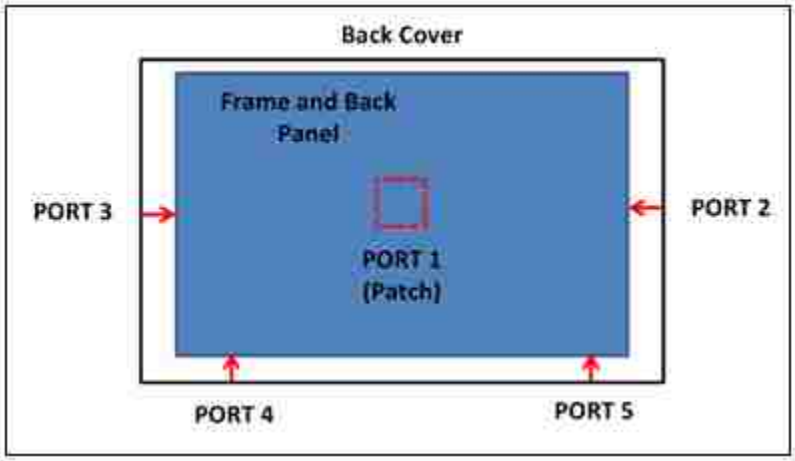

Figure 4.12. Components modeled

Figure 4.13 shows the measurement condition showing the metal patch excitation.

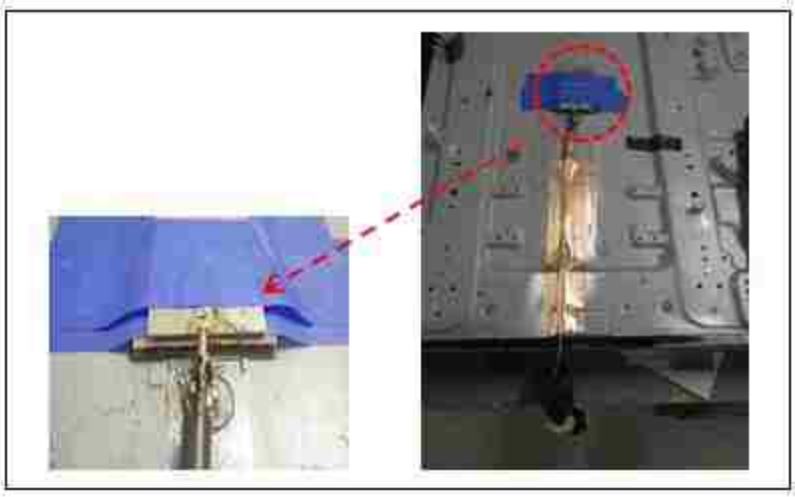

Figure 4.13. Measurement condition showing metal patch excitation

Figure 4.14 shows the simulation model.

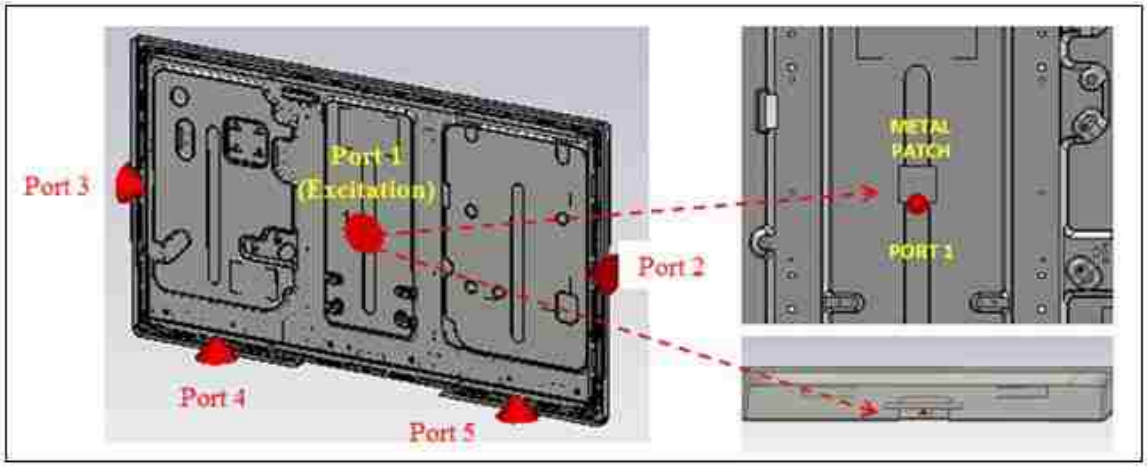

Figure 4.14. Simulation model

Figures 4.15, 4.16, 4.17, 4.18 show the simulation and measurement comparison for the s-parameters between port 1 (patch excitation) and port 2, port 3, port 4 and port 5 respectively.

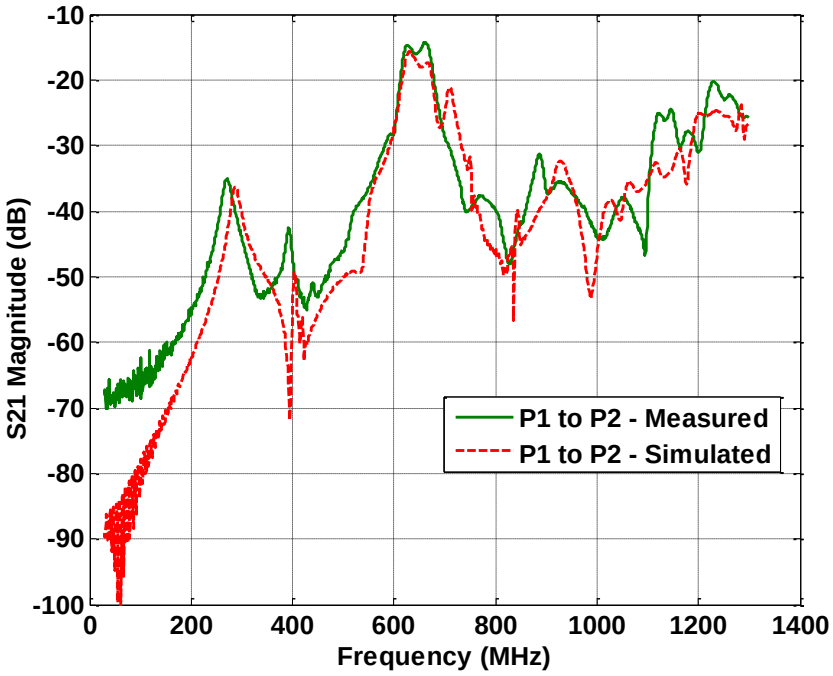

Figure 4.15. Simulation Vs Measurement for excitation ports 1 and 2.

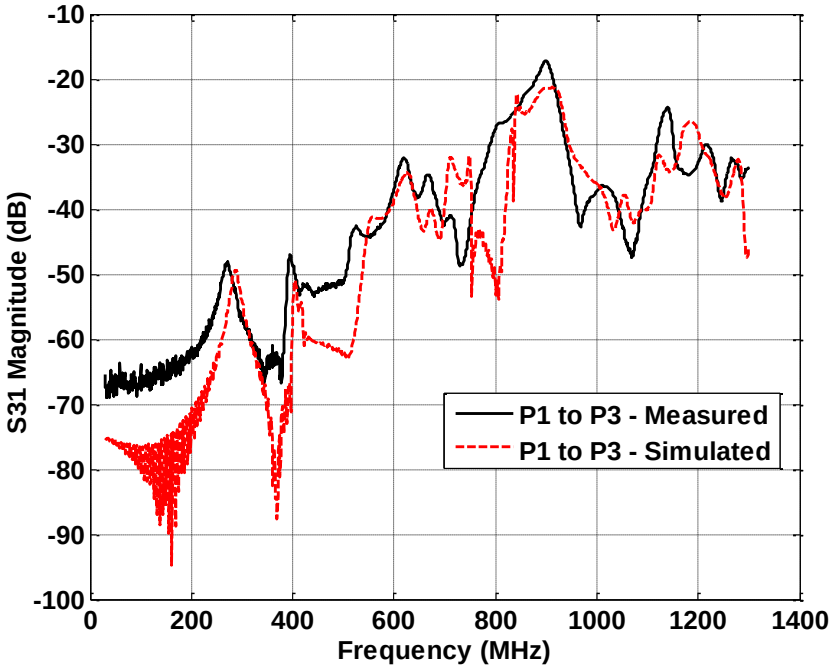

Figure 4.16. Simulation Vs Measurement for excitation ports 1 and 3.

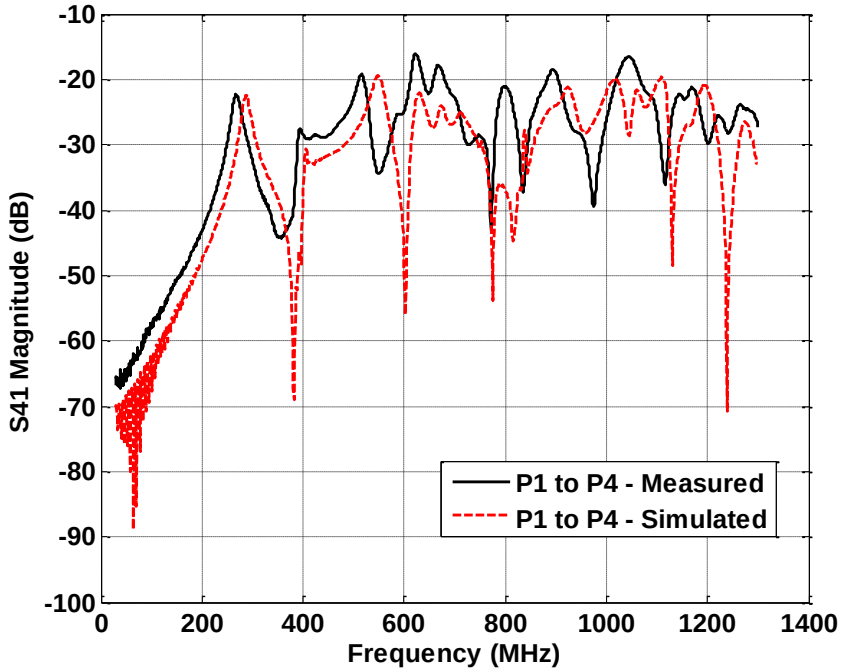

Figure 4.17. Simulation Vs Measurement for excitation ports 1 and 4.

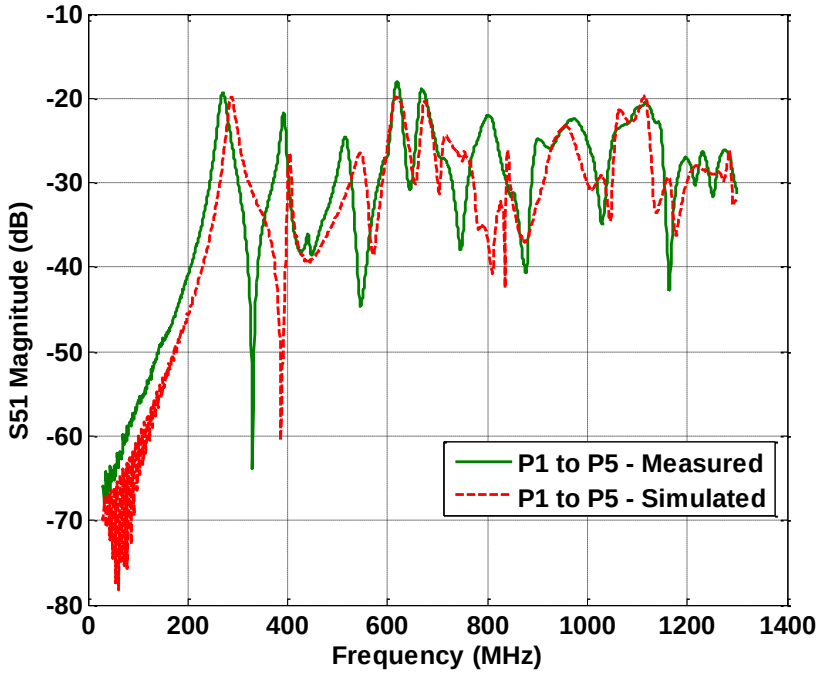

Figure 4.18. Simulation Vs Measurement for excitation ports 1 and 5.

4.2.6. Far-Field Validation of Chassis. The chassis model is validated for an excitation source present within the chassis. To validate this, a small 3cm X 3cm metal patch is used to excite the back panel. The measurement is done in a 3m anechoic chamber. The measuring antenna is kept at a distance of 3m from the chassis. In the simulation model, four far-field probes are places 3m away from the chassis. The simulation model setup is shown in the Figure 4.19.

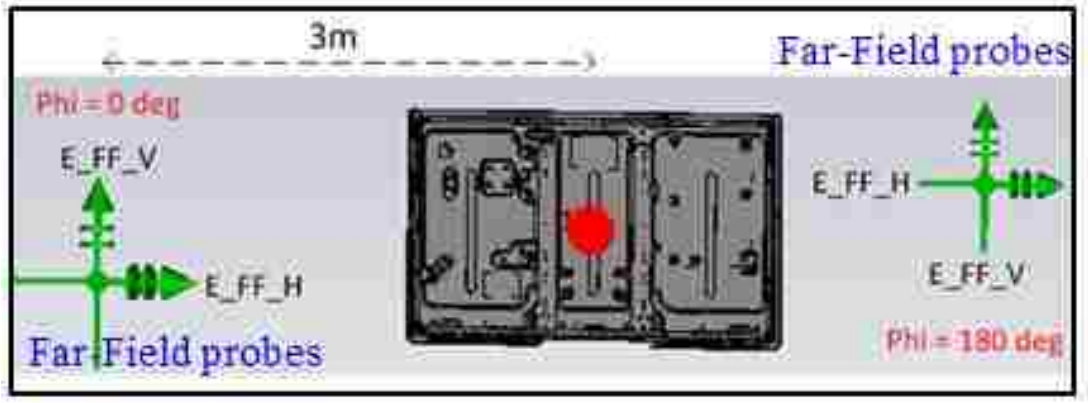

Figure 4.19. Far-field probes in simulation

Figure 4.20 shows the TV orientation for the measurement and the simulation.

Figure 4.20. TV Orientation

Figure 4.21 shows the comparison between the far-field emissions for the simulation and the measurement.

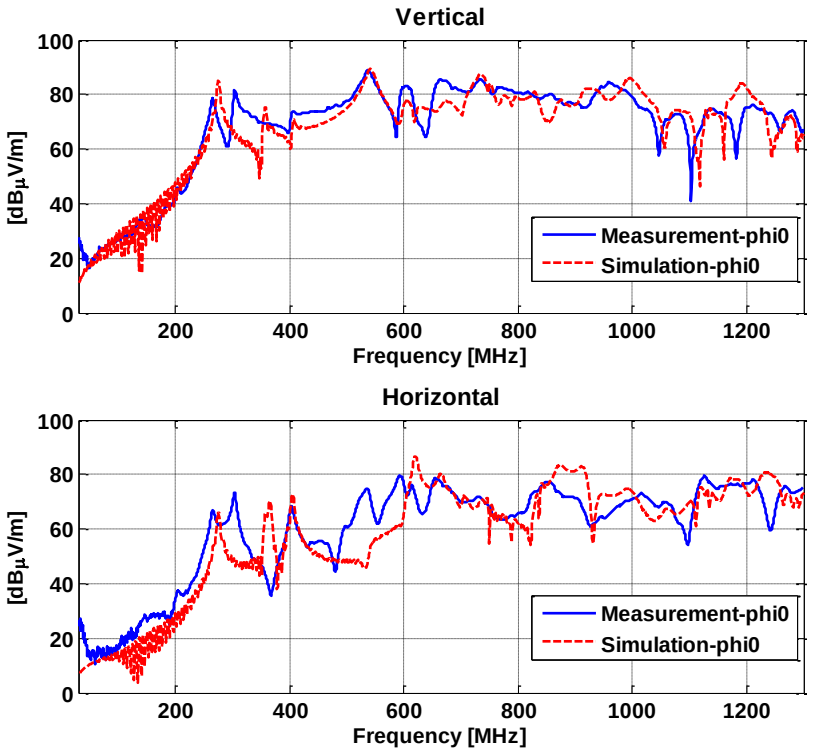

Figure 4.21. Simulation Vs Measurement for PHI=180 degrees

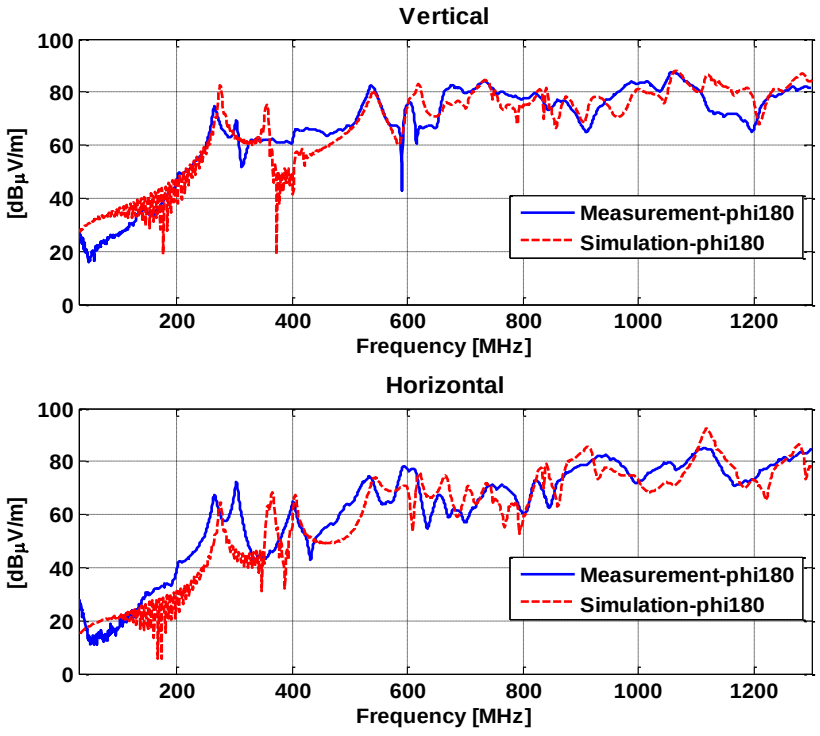

Figure 4.22. Simulation Vs Measurement for PHI=0 degrees

4.3. MAIN BOARD MODELING

The main board is modeled as a copper sheet with a FR-4 dielectric layer. Two ports are connected between the main board ground and the back panel. The dielectric thickness is parametrically varied in the simulation model to match the measured s-parameters of the measured main board.

Figure 4.23 shows the measurement on the main board.

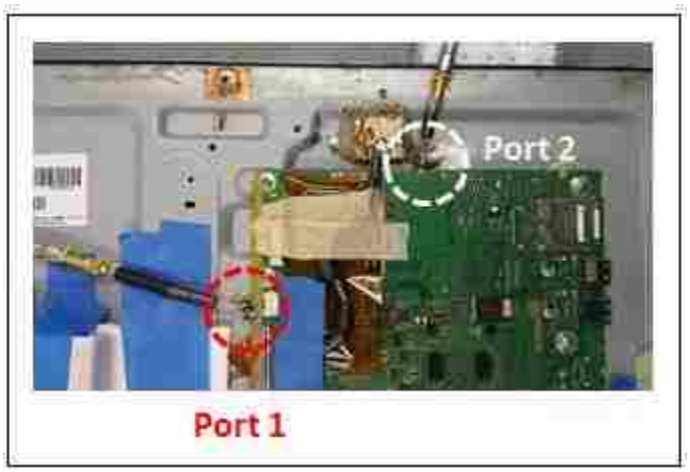

Figure 4.23. Measured main board.

Figure 4.24 shows the simulation model of the main board with a 0.6 mm dielectric layer. The dielectric layer thickness of 0.6 mm was obtained by parametrically varying the thickness such the simulated s-parameters matched the measurement result.

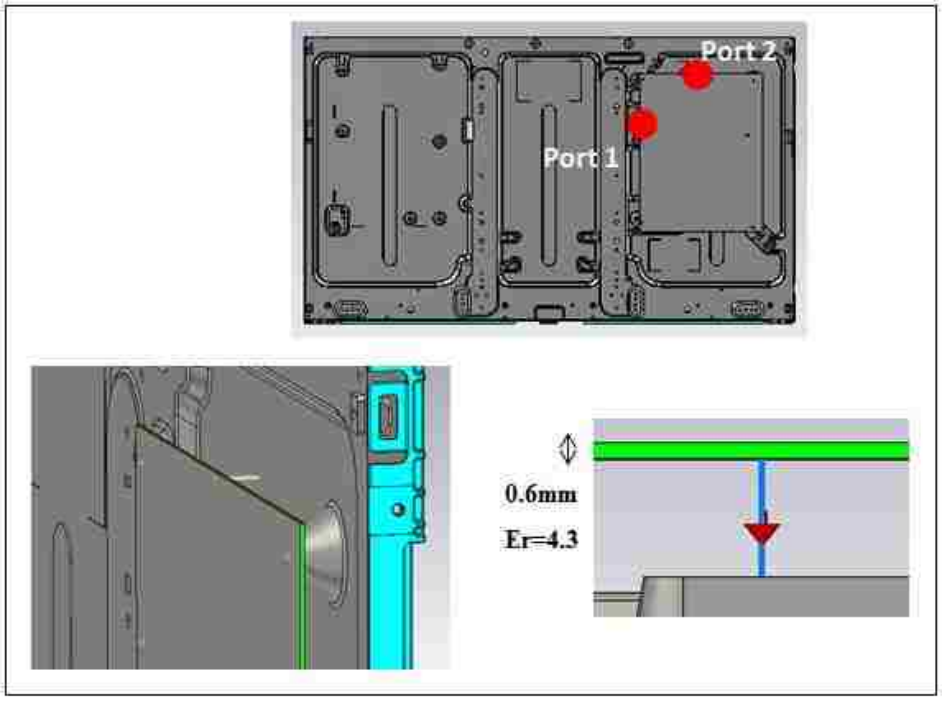

Figure 4.24. Simulation model

Figure 4.25 shows the simulation and measurement comparison for S_{11}(magnitude).

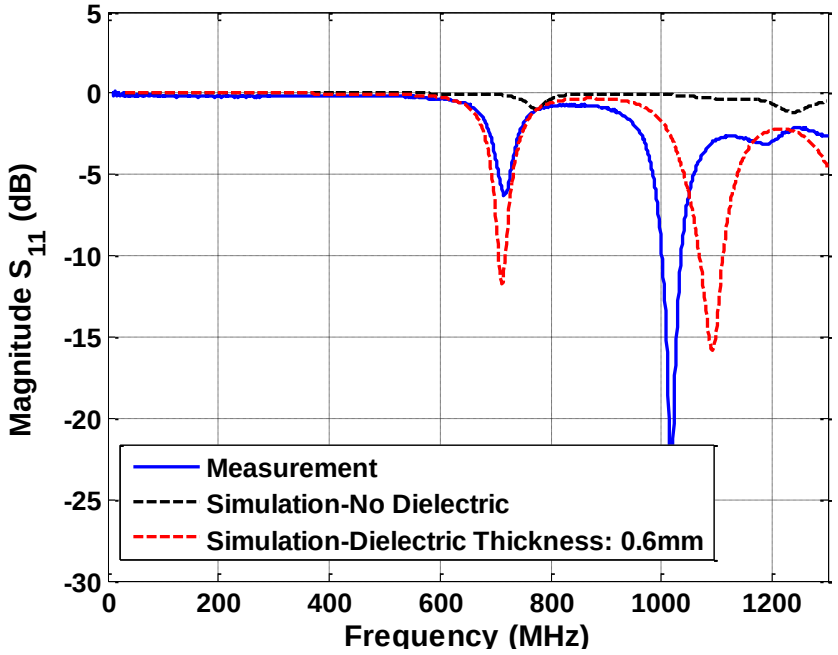

Figure 4.25. Simulation Vs Measurement

Figure 4.26 shows the simulation and measurement comparison for S_{21}(magnitude).

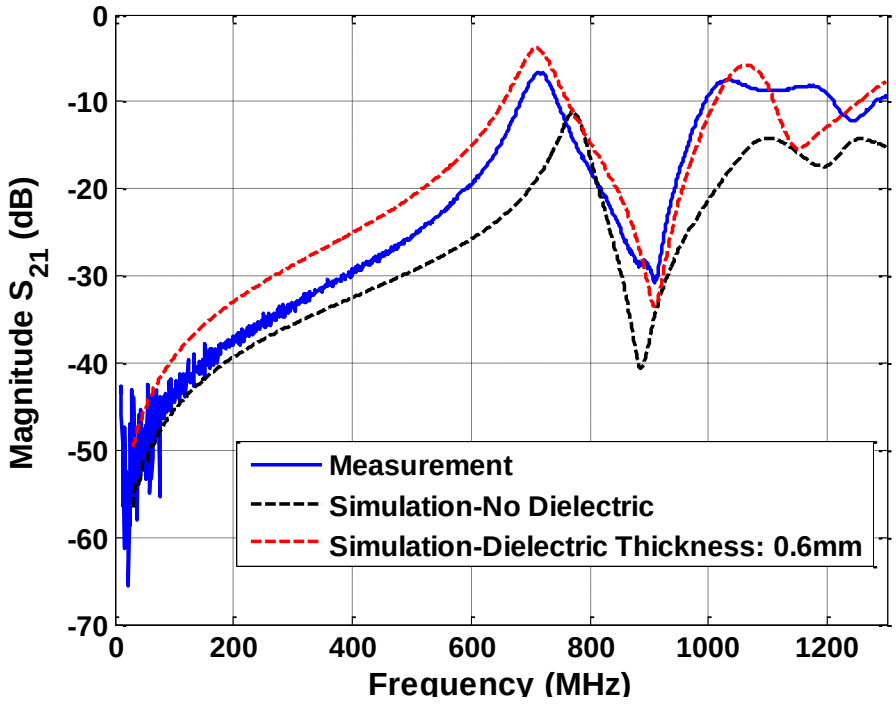

Figure 4.26. Simulation Vs Measurement

Figure 4.27 shows the measurement on the main board for different port locations.

.

Figure 4.27. Measured main board

Figure 4.28 shows the simulation model of the main board with a 0.6 mm dielectric layer.

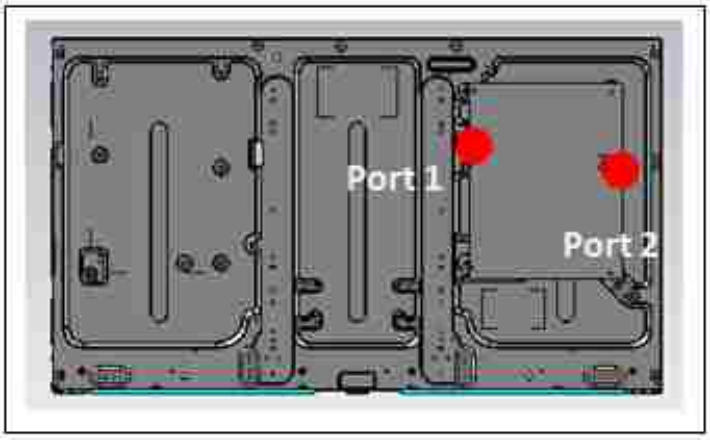

Figure 4.28. Simulation model

Figure 4.29 shows the simulation and measurement comparison for S_{11}(magnitude).

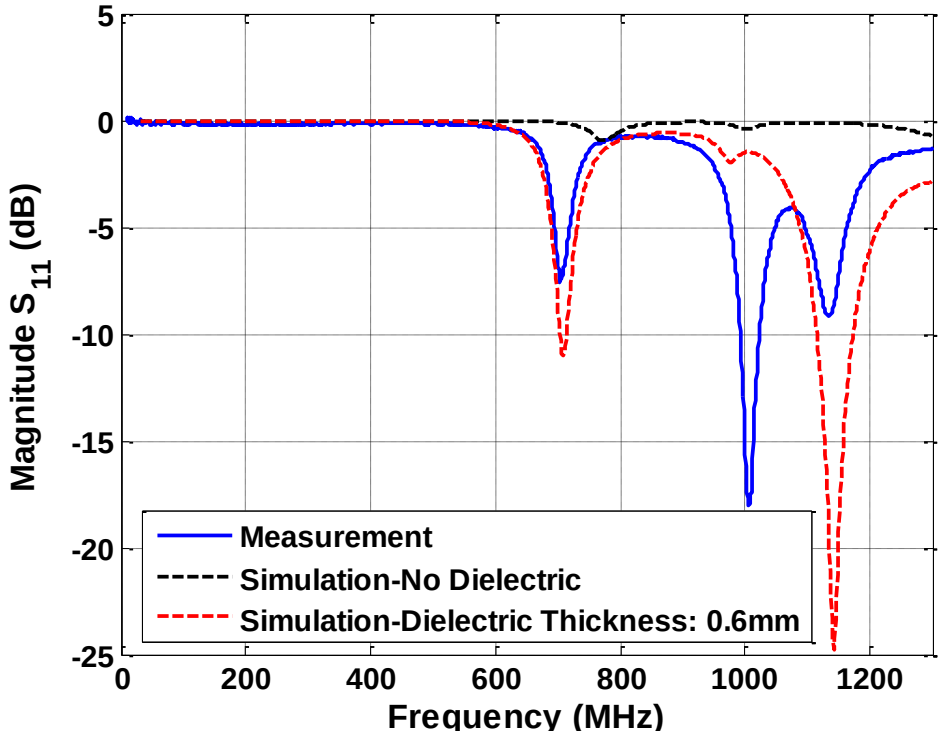

Figure 4.29. Simulation Vs Measurement

Figure 4.30 shows the simulation and measurement comparison for S_{21}(magnitude).

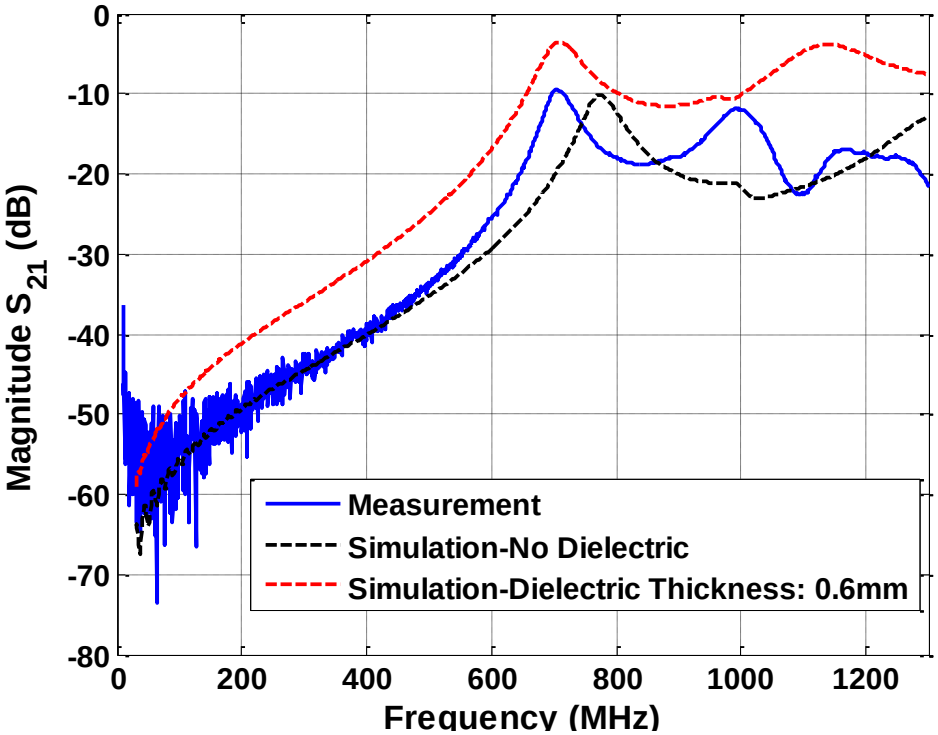

Figure 4.30. Simulation Vs Measurement

4.4. FLEX CABLE MODELING

Flex cables carry the display signals from the main board to the display driver board. Measurements indicate noise coupling from the flex cables to the chassis depending on flex position over the back panel. Change in coupling to chassis, causes change in radiated emissions.

Figure 4.31 shows the dimensions of the flex cable.

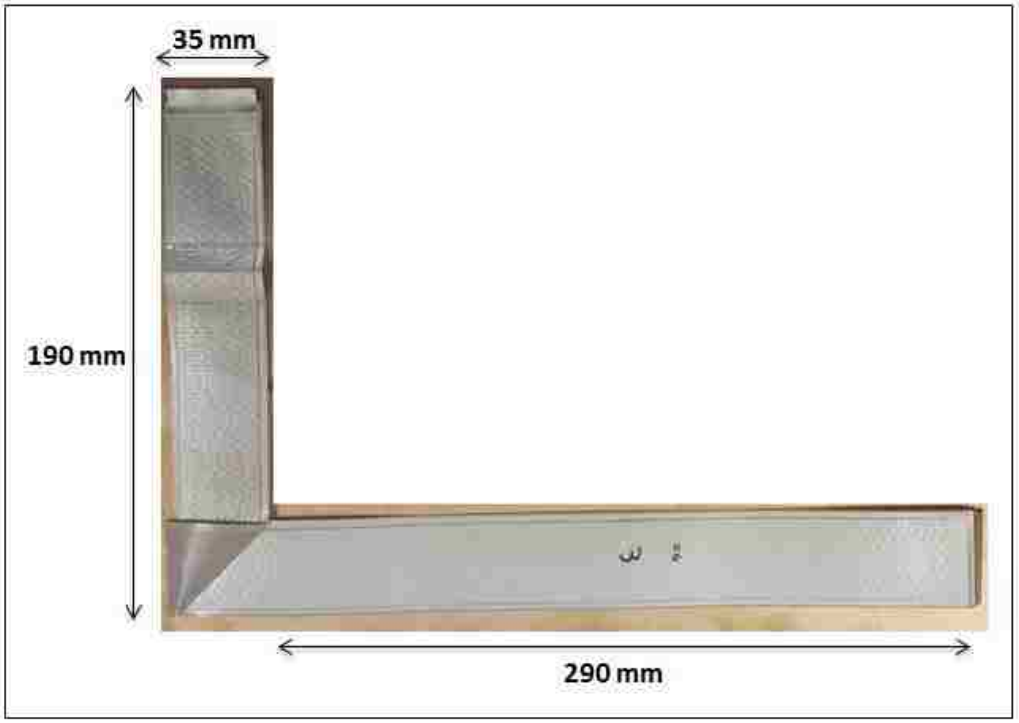

Figure 4.31. Flex cable dimensions

Figure 4.32 shows the flex cable stack-up obtained from the cross-sectional analysis

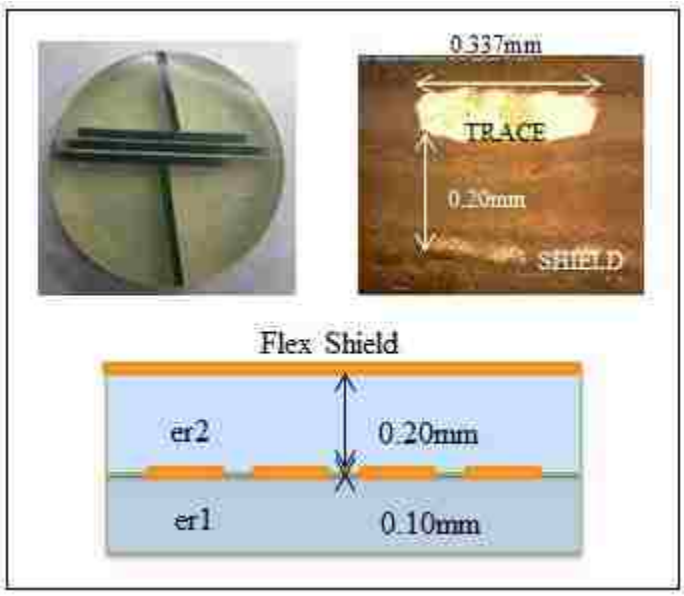

Figure 4.32. Flex cable stack from the measured cross-section

The frequency response of the flex cable over the copper sheet (emulating back panel) is measured for validating the simulation model of the flex cable.

Figure 4.33 shows the measurement setup for the flex cable s-parameters.

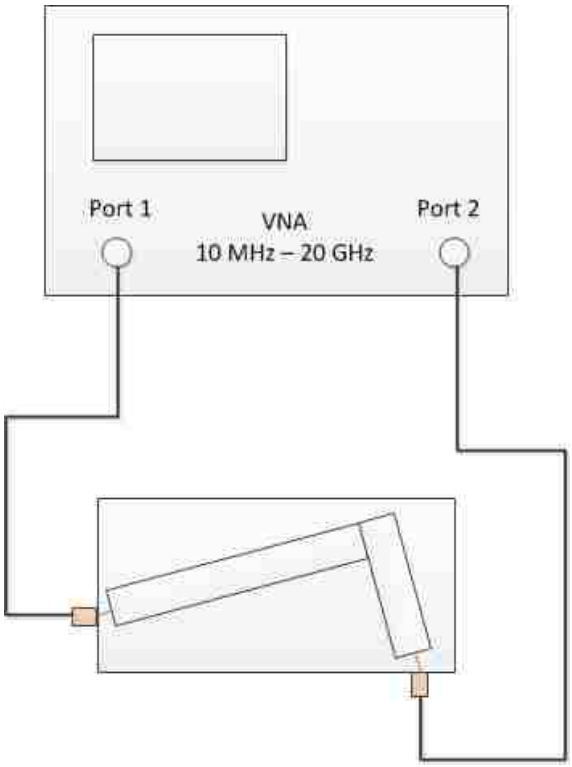

Figure 4.33. Measurement Setup

Figure 4.34 shows the flex cable placed over a copper sheet (emulating the back panel) for measurement of the s-parameters.

Figure 4.34. Flex cable over copper sheet

Figure 4.37 shows the simulation model of the flex cable with the flex fold region

- The flex cable is modelled with two signal and two ground traces.
- Four ports are used for the excitation.
- Two dielectric layers are used.

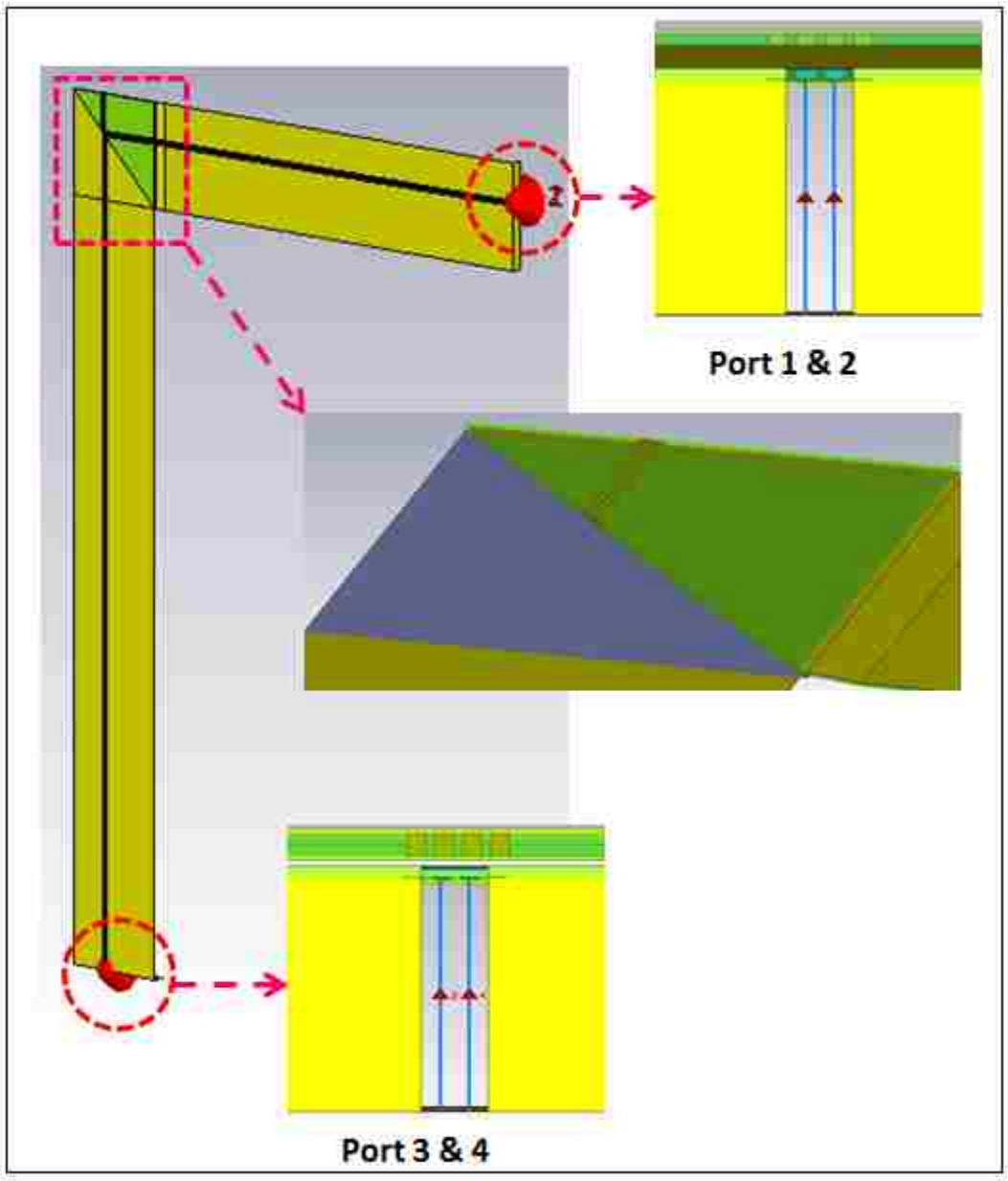

Figure 4.35. Simulation model

Figure 4.36 shows the ADS model used to obtain the common mode s-parameters from the 4-port measured and simulated s-parameters.

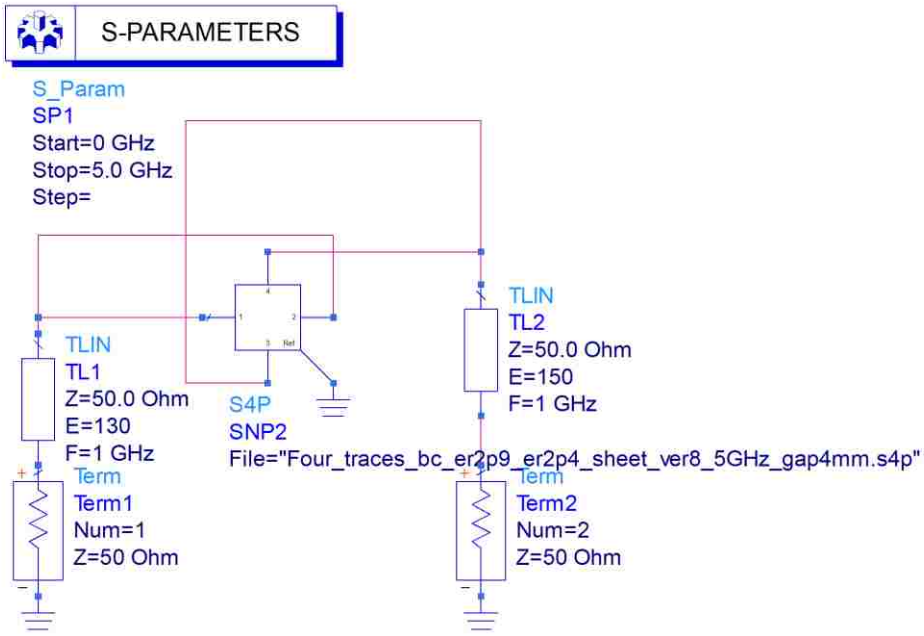

Figure 4.356. ADS model

4.4.1. Model Validation Part 1: Flex Cable 4 mm Above the Back Panel.

The Figure 4.37 shows the flex cable stack-up when it is 4 mm above the back panel. The back panel can be ignored.

Relative permittivities of the materials parametrically obtained are -

er1 = 2.9

er2 = 2.4

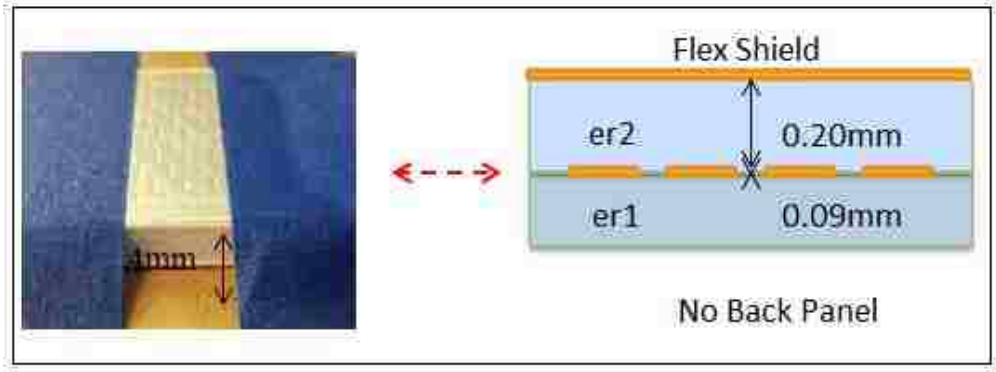

Figure 4.367. The flex cable 4 mm above the back panel

Figure 4.38 shows the simulation and measurement comparison for the impedance profile for the flex cable looking into from port 1 & 2.

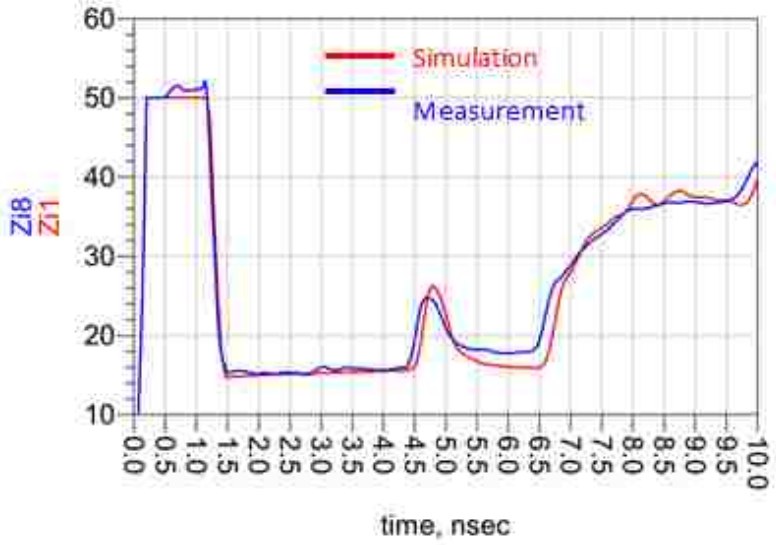

Figure 4.38. Simulation Vs Measurement

Figure 4.39 shows the simulation and measurement comparison for the impedance profile for the flex cable looking into from port 3 & 4.

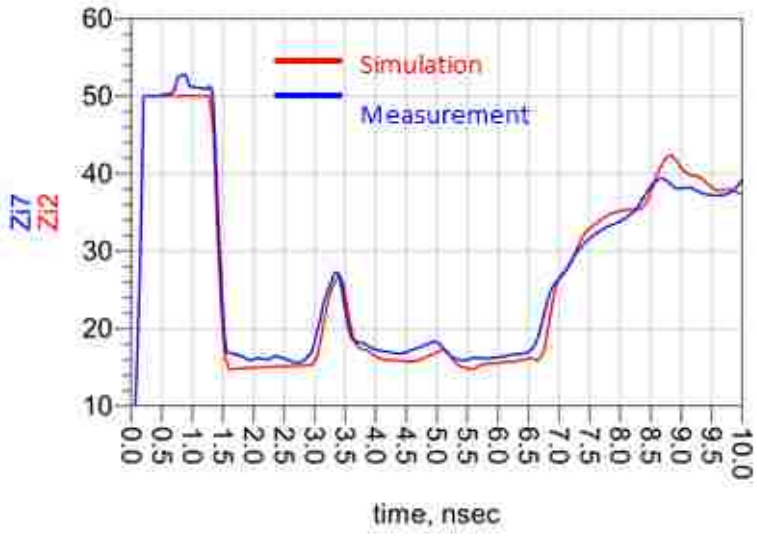

Figure 4.39. Simulation Vs Measurement

Figure 4.40 shows the simulation and measurement comparison of the Scc_{21}(magnitude) for the flex cable.

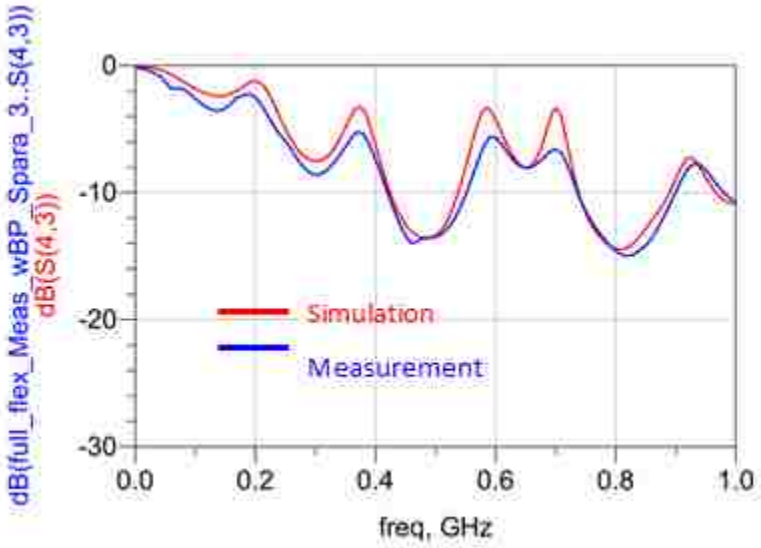

Figure 4.40. Simulation Vs Measurement

4.4.2. Model Validation Part 2: Flex Cable 0 mm Above the Back Panel.

The Figure 4.41 shows the flex cable stack-up when it is 0 mm above the back panel.

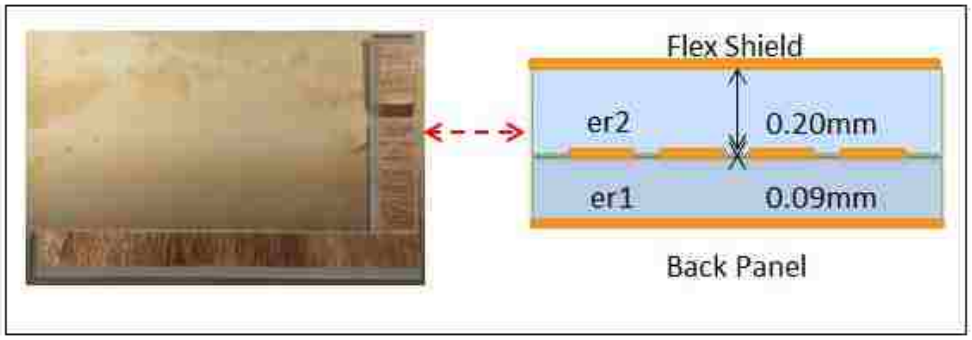

Figure 4.41. The flex cable 0 mm above the back panel

Figure 4.42 shows the simulation and measurement comparison for the impedance profile for the flex cable looking into from port 1 & 2.

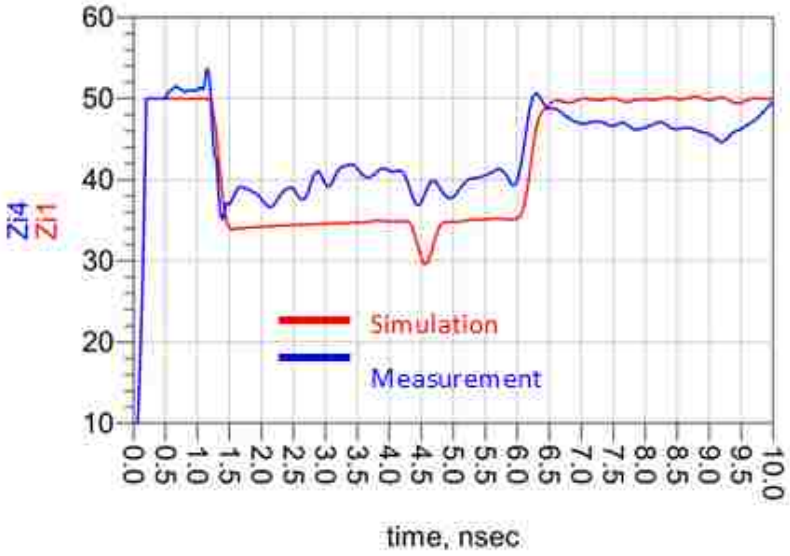

Figure 4.42. Simulation Vs Measurement

Figure 4.43 shows the simulation and measurement comparison for the impedance profile for the flex cable looking into from port 3 & 4.

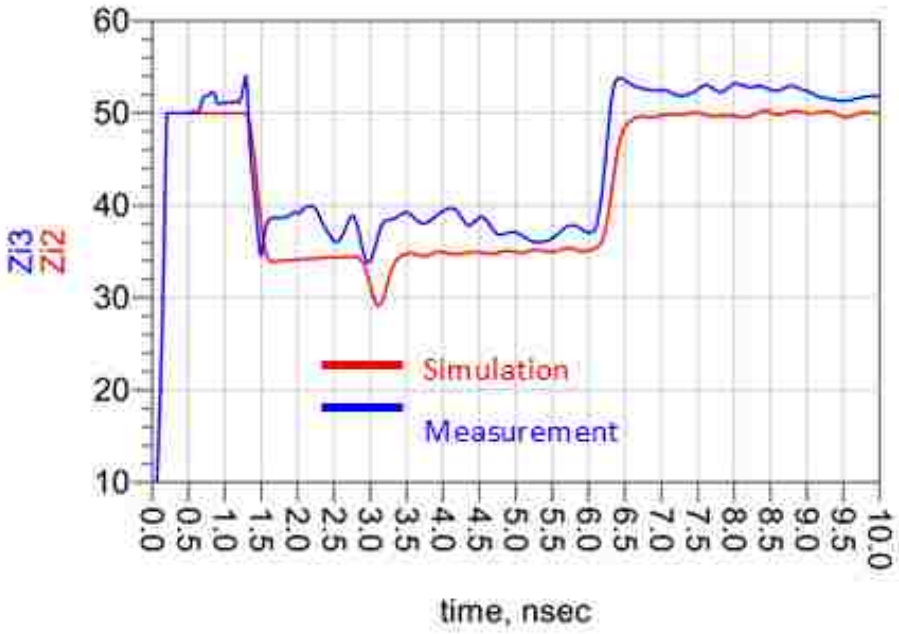

Figure 4.37. Simulation Vs Measurement

Figure 4.44 shows the simulation and measurement comparison of the Scc_{21}(magnitude) for the flex cable.

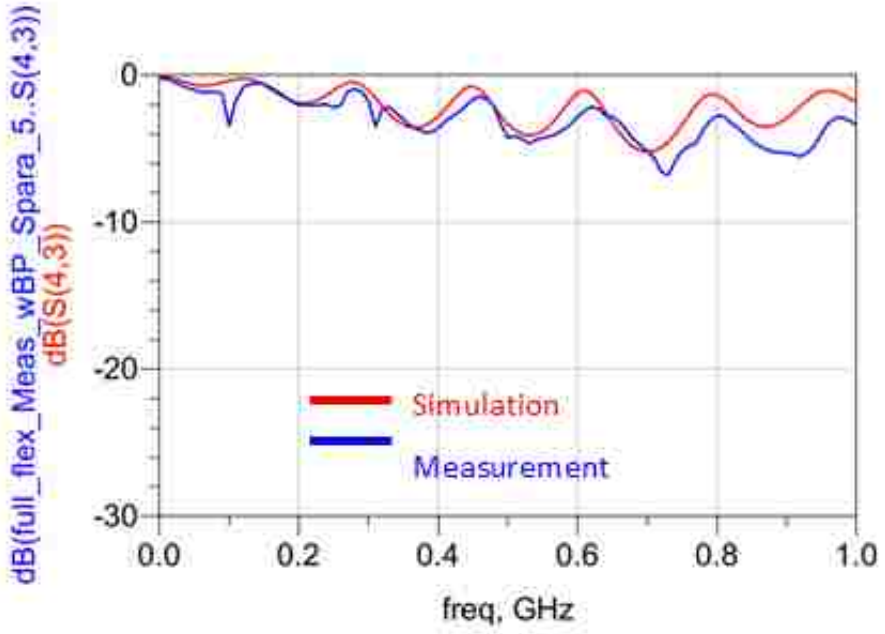

Figure 4.4. Simulation Vs Measurement

4.4.3. Flex Cable Modeling: Variations Between Different Flex Cables.

Variations in the characteristics have been observed for different flex cables from the same manufacturer. One flex cable characteristics were used as reference for the flex cable model validation.

Figure 4.45 shows the two flex fables from the same manufacturer.

Figure 4.385. Two Flex Cables from the same manufacturer

Figure 4.46 shows the measured TDR response without copper sheet (Back Panel). The results shows variations in the impedance between the two cables.

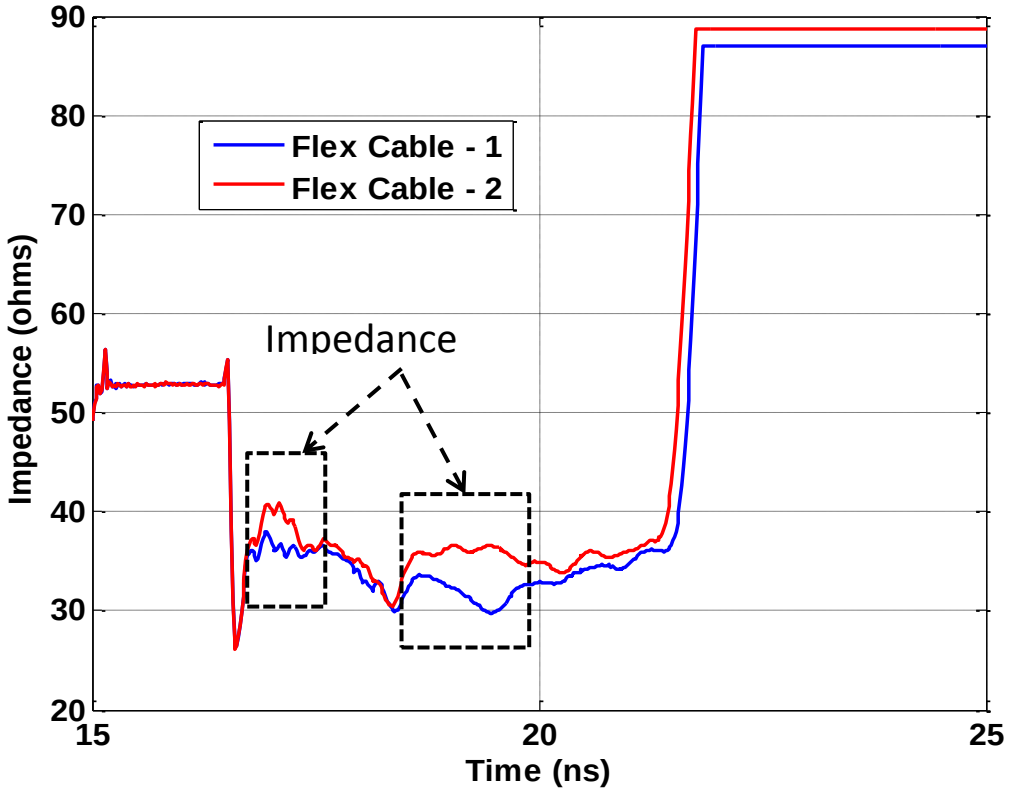

Figure 4.396. Measured TDR response for the two flex cables without copper sheet (Back Panel)

4.5. DISPLAY DRIVER BOARD MODELING

A substitution display driver board was constructed for measurements without the display panel and modeling the driver board. The substitution driver board retained the parts of the original driver boards that might influence the electromagnetic characteristics of the interaction of the board with the chassis. Figure 4.47 shows the original driver board and the substitution boards with the similar parts.

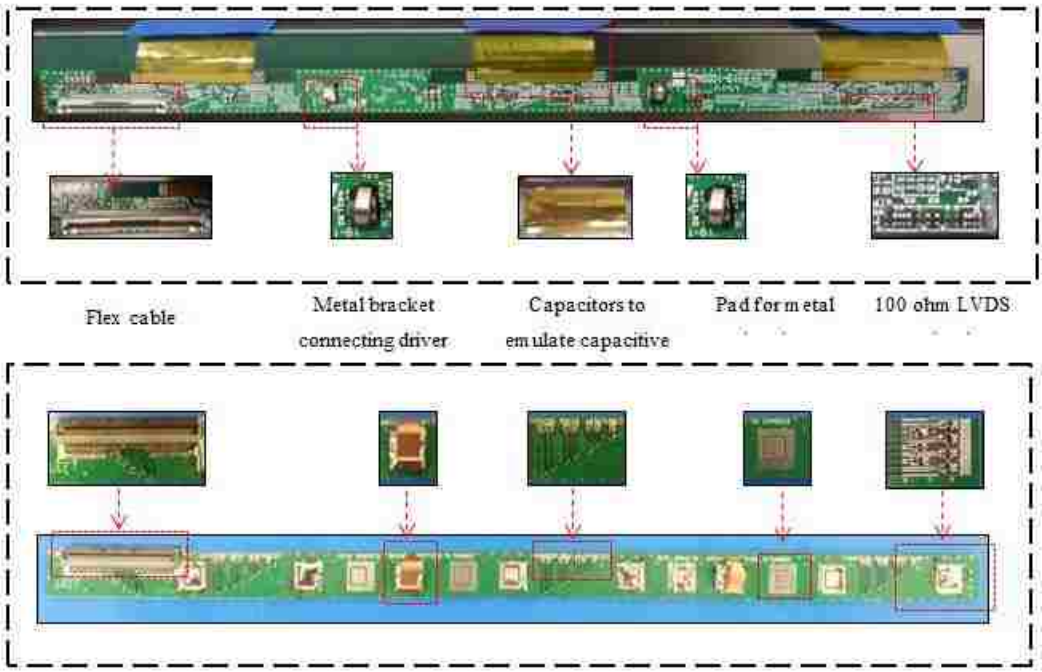

Figure 4.407. Original display driver board and substitution driver board

The substitution driver board model was created as a two layer board with the differential pair on one side. The stack-up of the board is as shown in Figure 4.48.

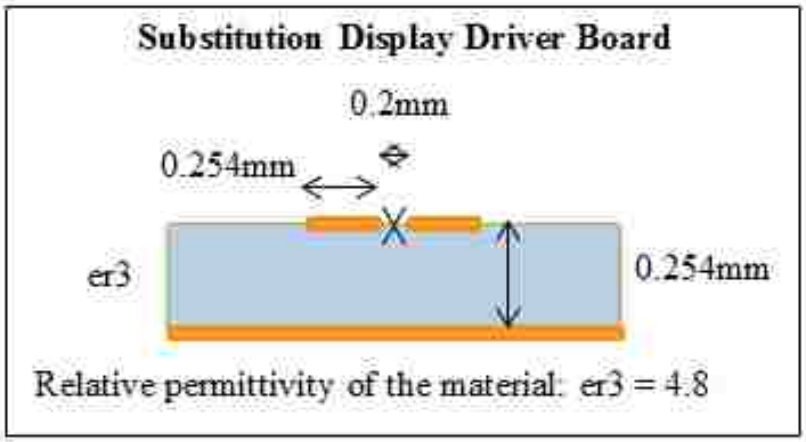

Figure 4.48. Substitution display driver board cross-section

To validate the driver board model, coupling from the driver board ground to the back panel upon common mode injection into the differential trace pair is modeled. Two ports were connected – port 1 excites the differential trace pair in common mode with the back panel as a reference. The port 2 is connected from the driver board ground with the back panel as a reference.

The simulation model with the port locations is shown in Figure 4.49.

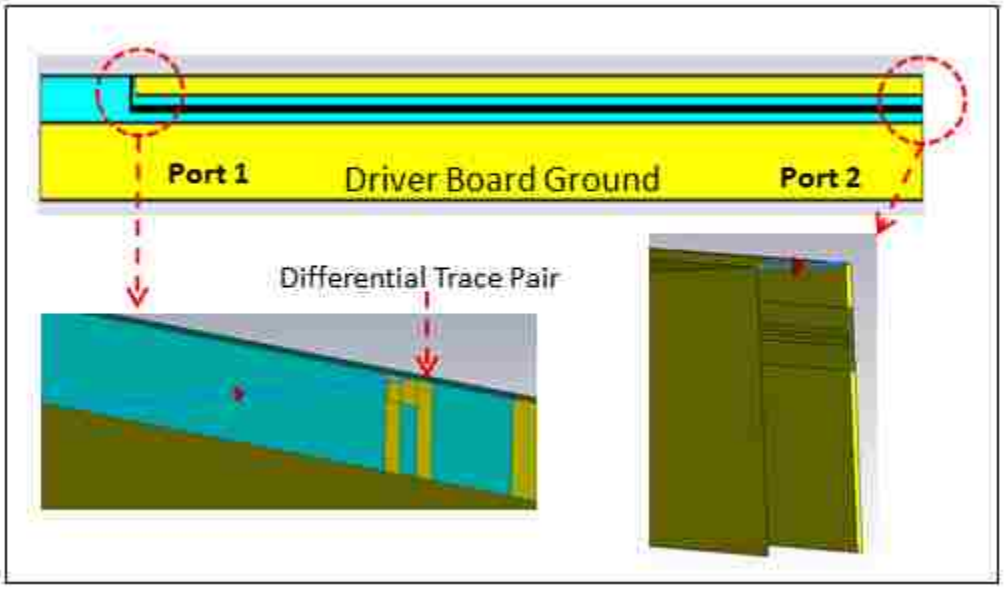

Figure 4.49. Simulation model of the driver board.

The measurement setup with the port locations is shown in Figure 4.50.

Figure 4.50. Measurement setup

Figure 4.51 shows the comparison between the simulated and measured s-parameters for the driver board.

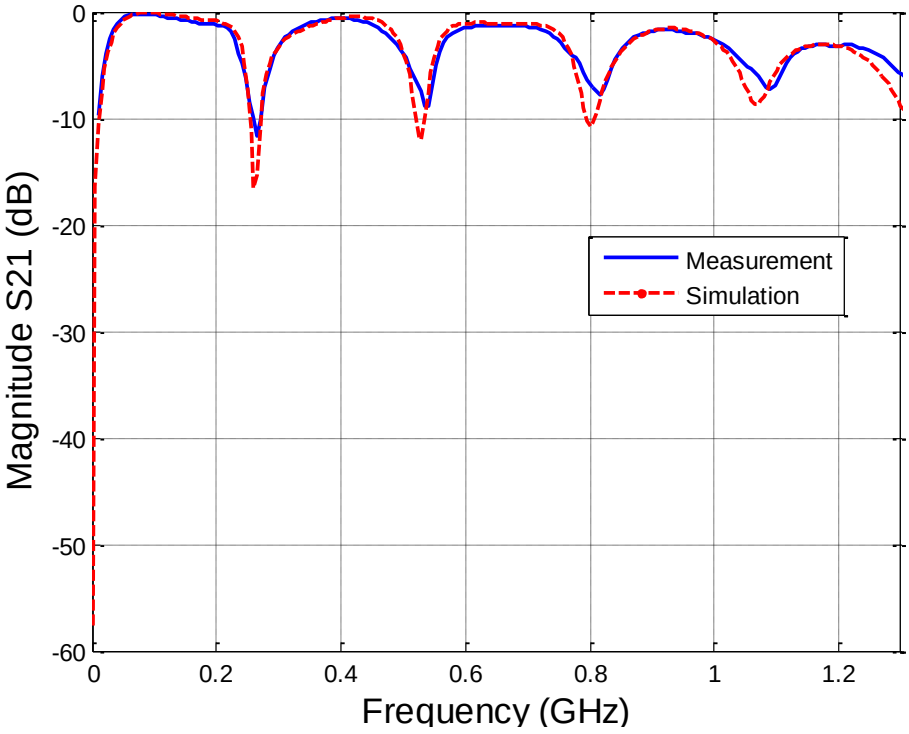

Figure 4.51. Simulation Vs Measurement

5. COMMON MODE MODEL

5.1. COMMON MODE MODEL DESCRIPTION

The common mode model consists of only the return/reference structures of the components.

5.2. NEED FOR THE COMMON MODE MODEL

The common mode model can be useful for -

- Faster verification of the complete model.
- Identification of resonant structures.
- It can predict coupling and radiation characteristics of chassis components.
- The radiated emissions can be correlated to certain common mode structures.

The far-field measurement setup for the common mode model is shown in Figure 5.1.

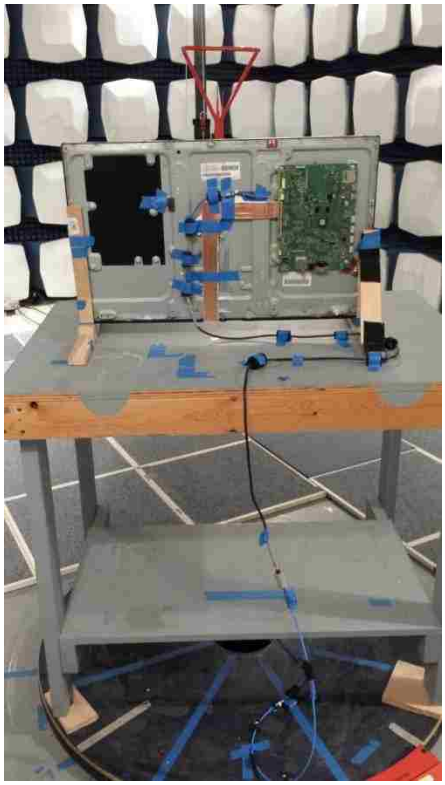

Figure 5.1 Measurement setup

The far-field radiations predicted from the simulation models are validated with measurements by adding components one by one and comparing the simulated results with the one measured. The analysis of the radiation from addition of components one by one yields the resonant frequencies for the components and the change in the resonances due the addition of the next component. This helps to gain a better understanding of the coupling and radiation mechanisms. Figure 5.2 shows the common mode model validation steps.

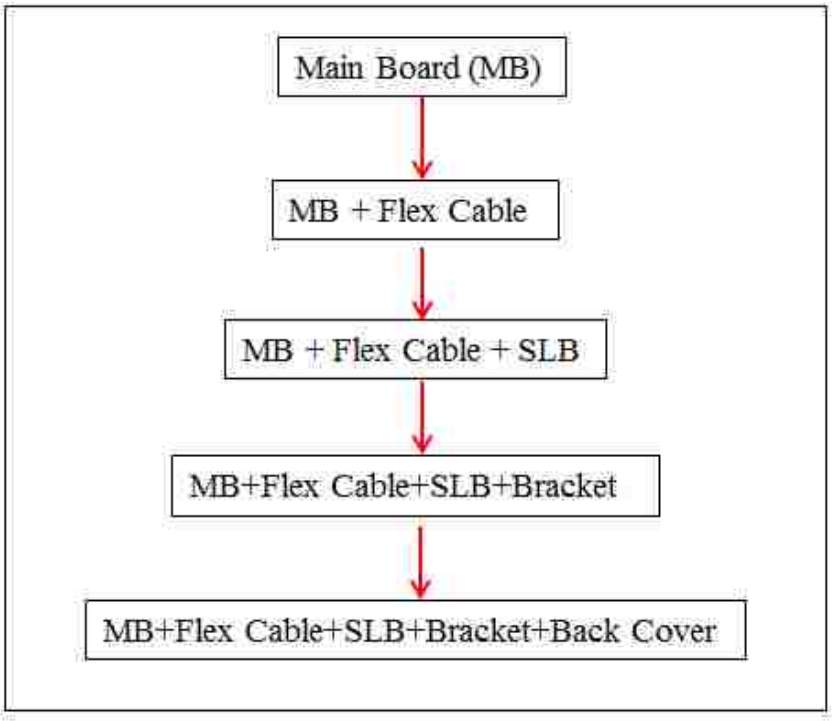

Figure 5.2. Model validation steps

Figure 5.3 shows the components modeled.

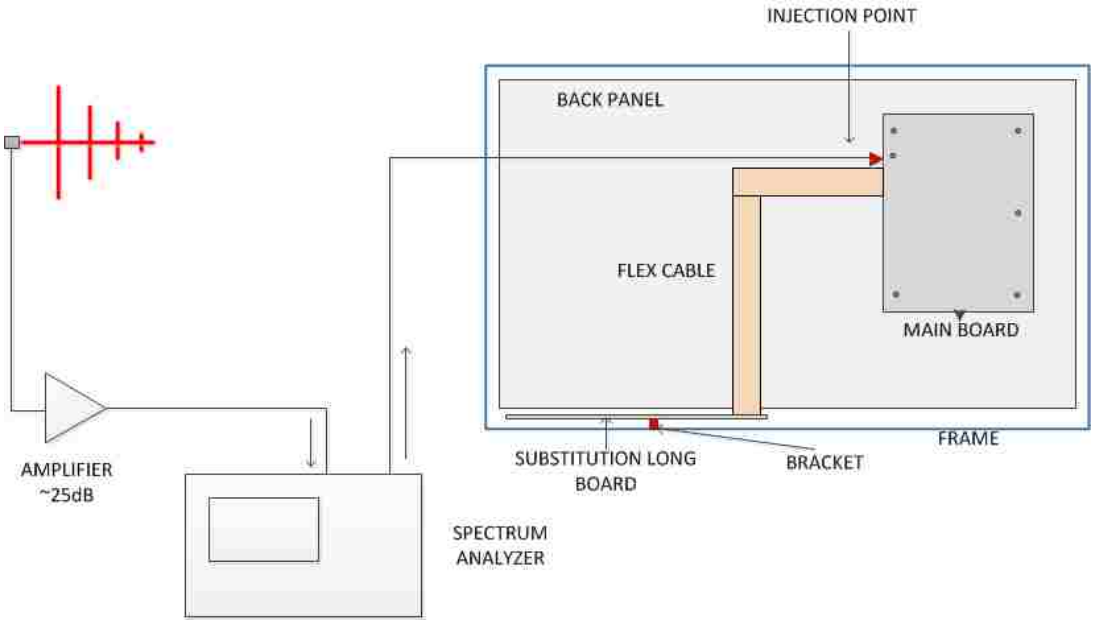

Figure 5.3. Measurement setup

Figure 5.4 shows the port location in the simulation model.

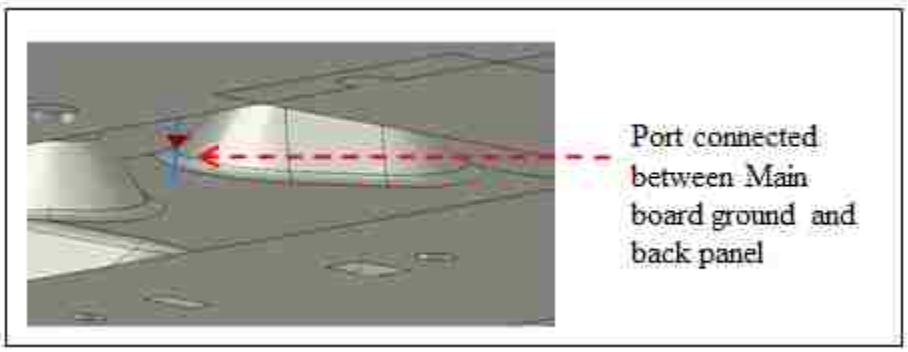

Figure 5.4. Port location in simulation model.

Figure 5.5 and 5.6 show the comparison between the far-field result for the simulation model and the measurement.

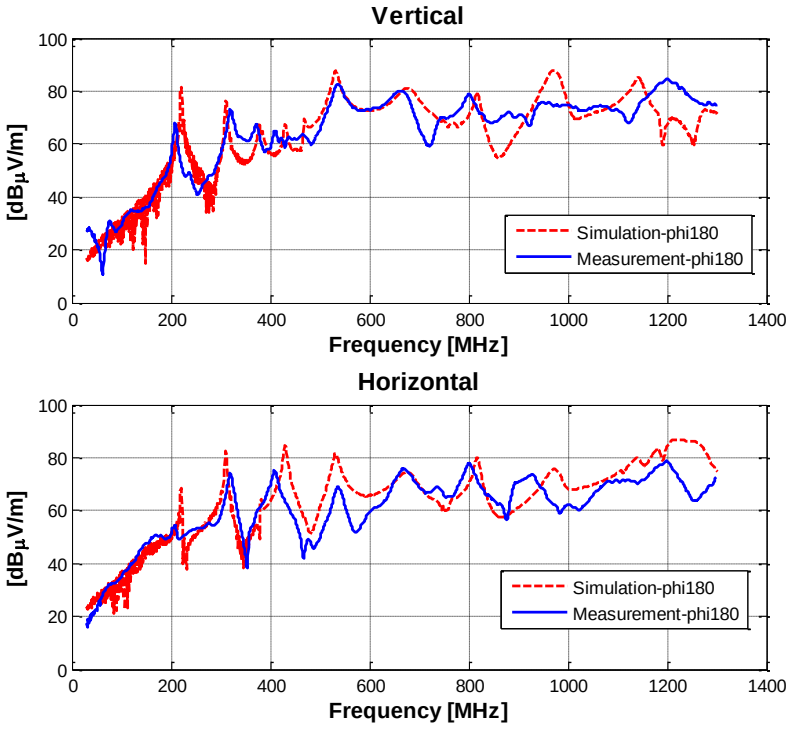

Figure 5.5. Simulation Vs Measurement for Phi=180 degrees

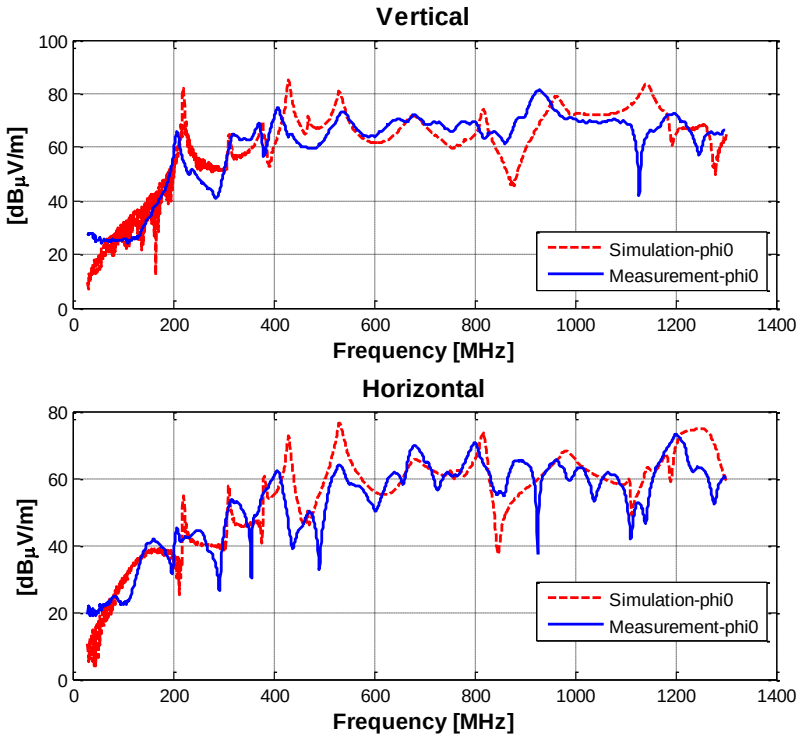

Figure 5.6. Simulation Vs Measurement for Phi=0 degrees

5.3. FLEX POSITION CHANGE OVER BACK PANEL

In the actual TV, the separation between the flex cable and the back panel can vary over the length of the flex cable. To validate our common mode model to check such a condition of the flex cable, we introduce a bend region in the flex cable both in the measurement and the simulation model.

The bend in the measurement is shown in Figure 5.6. The bend region is at a height of 0.8 mm above the back panel.

Figure 5.7. Flex cable bend region 0.8 mm above the back panel

Figures 5.8 and 5.9 show the comparison of the far-field for the simulation and the measurements for the back side (phi=180 degrees) and front side (phi=0 degrees) radiation respectively.

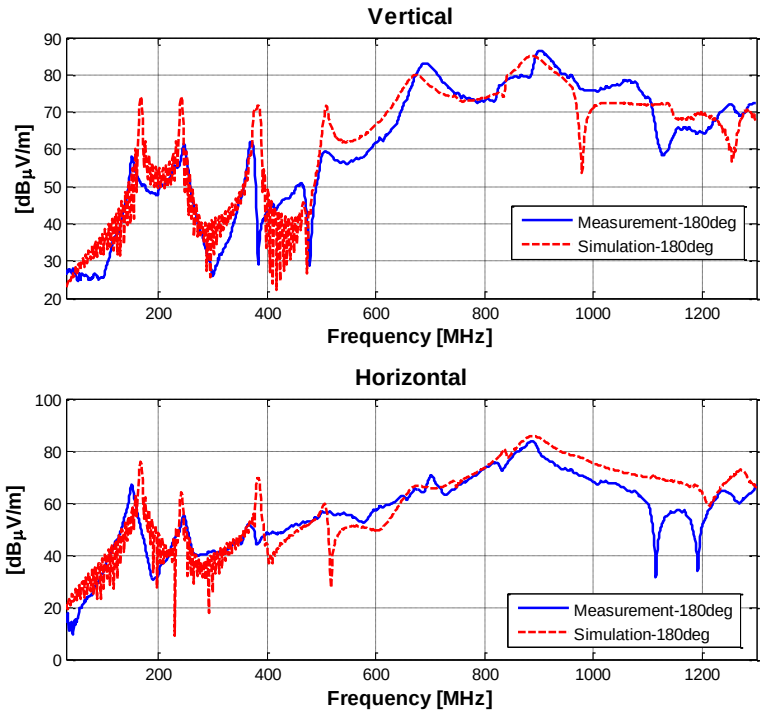

Figure 5.8. Simulation Vs Measurement for Phi=180 degrees

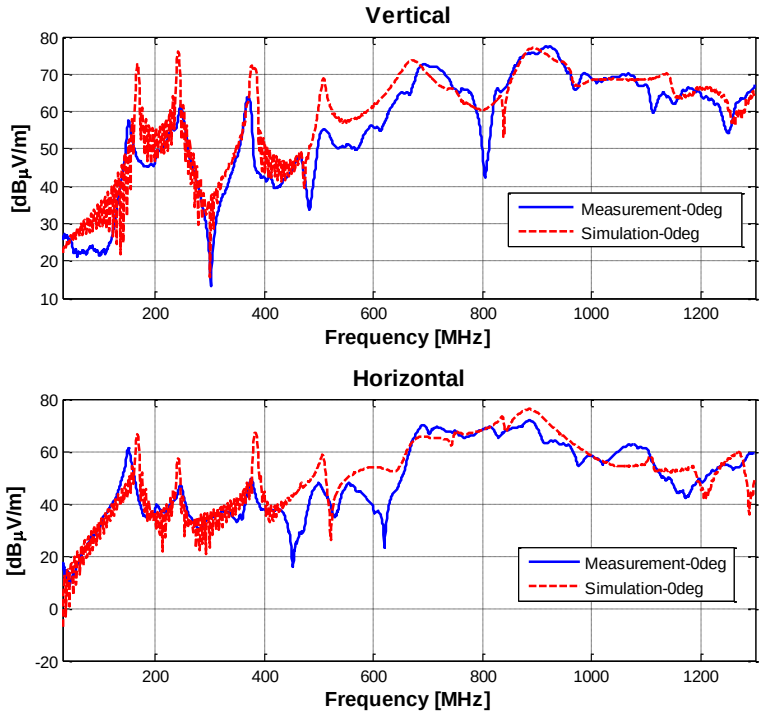

Figure 5.9. Simulation Vs Measurement for Phi=0 degrees

6. COMPLETE MODEL VALIDATION

The individual component models are combined to form the complete model of the TV. The excitation is via one lumped port into the differential trace pair with the main board ground as reference. The port 1 shown is the excitation port of the model. Far-field E-field probes are used at 3m away from the chassis in two opposite directions to obtain the radiated far-field at 3m in the front side (0 degree) and back side (180 degree) of the chassis. The flex slope regions in the middle region of the flex cable, the dimensions of which can be varied to analyze the effect of flex cable condition above the chassis. Over previous measurements on the live TV and common mode injection have indicated change in the gap voltages and the radiated emissions on the change in the position of flex cable above the chassis. Thus, to analyze this effect qualitatively and quantitatively, we can simulate this change using the simulation model shown in Figure 6.1.

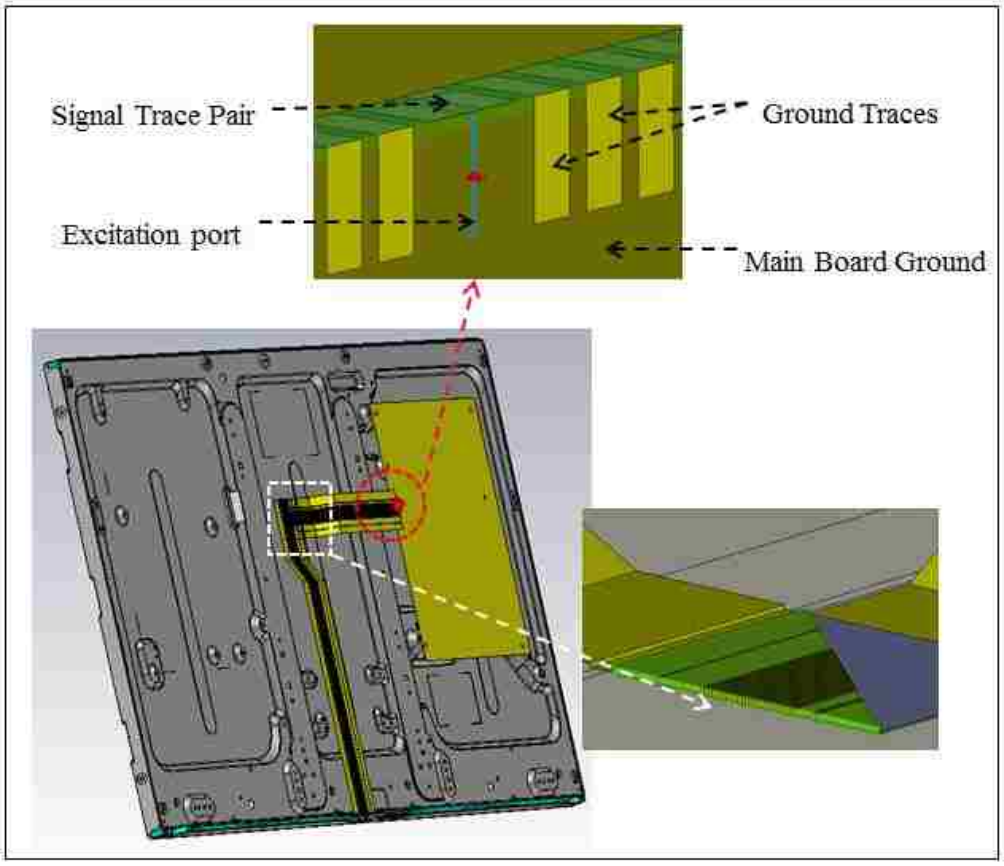

Figure 6.1. Complete simulation model of the flat panel display.

Figure 6.2 shows the flex fold region of the flex cable model.

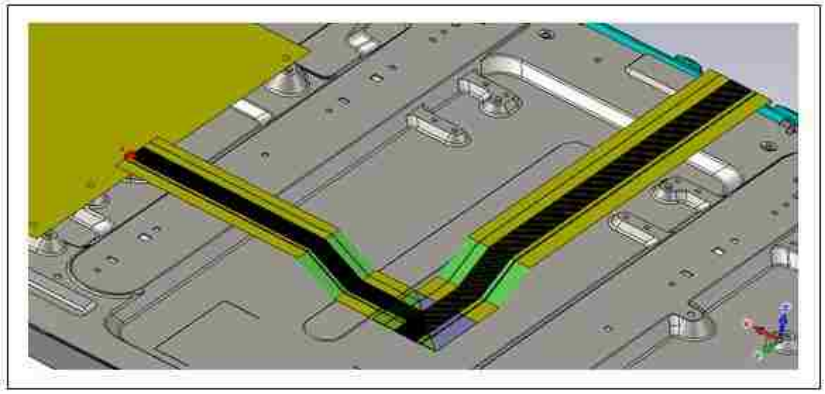

Figure 6.2. Flex fold region

Figure 6.3 shows the simulation and actual flex fold region used for the simulation and the measurement. The flex fold region is kept at a distance of 0.8 mm above the back panel.

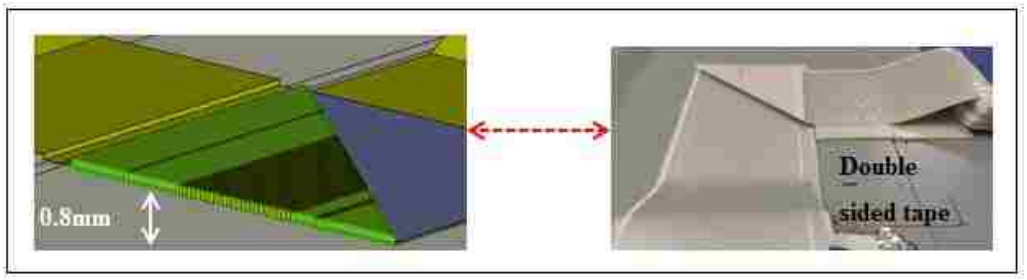

Figure 6.3. Flex fold region 0.8 mm above back panel

Figures 6.4 and 6.5 show the comparison of the far-field for the simulation and the measurements for the complete model without the back cover for the back side (phi=180 degrees) and front side (phi=0 degrees) radiation respectively.

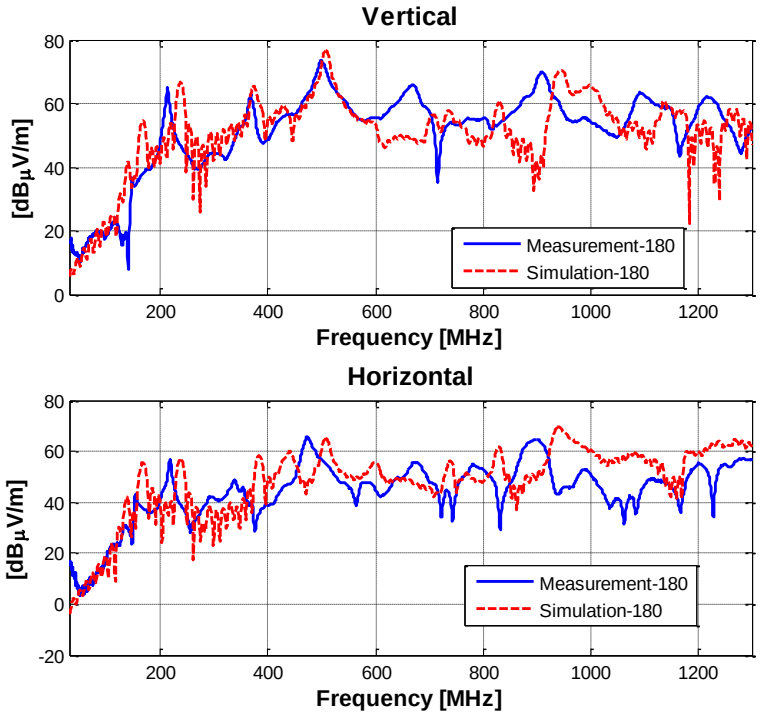

Figure 6.4. Simulation Vs Measurement for Phi=180 degrees

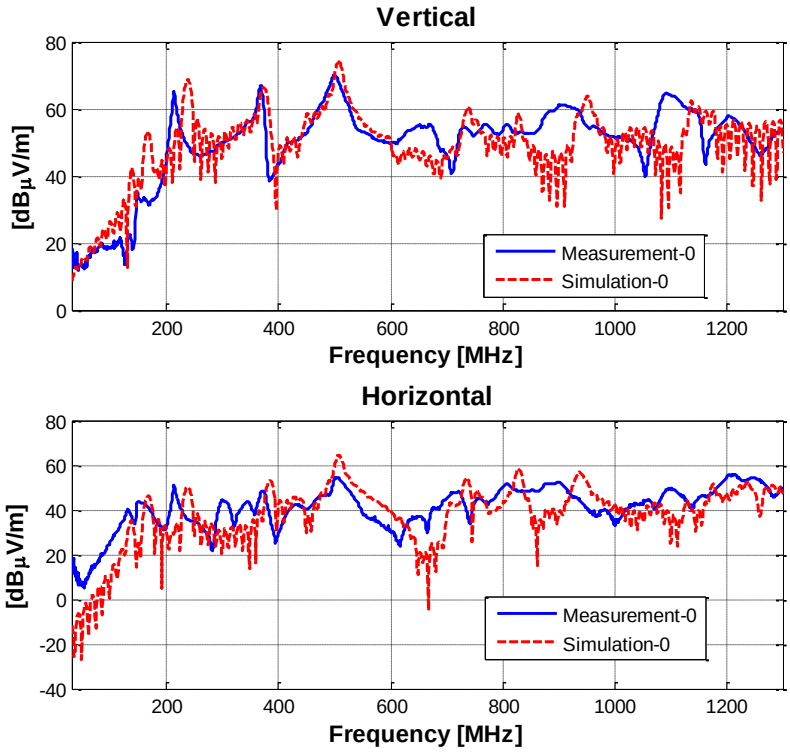

Figure 6.5. Simulation Vs Measurement for Phi=0 degrees

7. CONCLUSIONS AND FUTURE WORK

7.1. CONCLUSIONS

- Radiated emissions are dependent and highly sensitive to the condition of the flex cable over the back panel.
- Analysis of coupling paths based on measurements is difficult due to the presence of multiple resonances due to many electrically large components.
- The chassis components form antenna structures.
- The display panel itself does not contribute significantly to the radiated emissions.
- The display driver boards are responsible for the resonances are low frequencies (60 – 120 MHz).
- Different flex cables from same manufacturer might have different characteristics.
- Measurements require opening the chassis, which changes the actual coupling mechanisms and radiation.
- The modeling approach for products with a large chassis is demonstrated.
- Individual components have been modeled using full-wave simulation tool – CST MWS.
- The dependence of radiation characteristics on the flex cable position over the back panel is shown in measurement and also predicted using the simulation model.

7.2. FUTURE WORK

- Use differential clock with known skew as a source to excite the complete model and compare the far-field spectrum with the one measured for the baseline measurement for TV.
- Analyze the noise coupling mechanism under various chassis and flex conditions and test feasible EMI reduction techniques using the full-wave simulation model.

BIBLIOGRAPHY

[1] Theodore M. Zeeff, Todd H. Hubing, et al., "EMC Analysis of an 18" LCD Monitor." Electromagnetic compatibility Symposium, IEEE 2000.

[2] Do-wan Kim, On-Sik Choi, et al.," The Effectiveness of Bulk Gasket and Shield Cover on the Reduction of EMI Radiation in LCD TV", Electromagnetic compatibility Symposium, IEEE 2005.

[3] Nansen Chen, Hongchin Lin, "A Two-Layer Board Intellectual Property to Reduce Electromagnetic Radiation.", Electromagnetic compatibility Symposium, IEEE 2010.

[4] Chang-Woo Ko, Young-Seok Hong, et al., "EMI Analysis of the LCD panel Considering the Display Driver IC Operations", Electrical Performance of Electronic Packaging Conference, IEEE 2005.

[5] Sung-Pil Choi, Jae Wook Kwon, et al., "EMI Analysis of TFT-LCD Driver IC", Electromagnetic Compatibility Symposium, IEEE 2006.

[6] Fumikazu Ga, Kengo Umeda, et al.," Electromagnetic Design Techniques for Liquid Crystal Display Driver ICs", Display Technology Journal, IEEE 2007.

[7] Do-wan Kim, On-Sik Choi, et al.," Chip level EMI approach for LCD TV panels.", Electromagnetic compatibility Symposium, IEEE 2007.

[8] Min-woo Kim, Do-wan Kim, et al.," Chip Level Techniques for EMI Reduction in LCD Panels", Electromagnetic Compatibility Symposium, IEEE 2009.

[9] Sung-Kyu Lee, Jung-man Lim, et al.," The Solutions of LCD Panel (T-Con) EMI Noise for Wireless Integration.", Electromagnetic compatibility Symposium, IEEE 2007.

VITA

Satyajeet Shinde was born in Pune, India. He received his B.E. degree from the University of Pune, Pune, India, in 2010. From 2010 to 2011, he was a Programmer Analyst Trainee in the Communications Testing Division, Cognizant, India. Since 2011, he has been a Graduate Research Assistant in the Electromagnetic Compatibility Laboratory, Missouri University of Science and Technology. He completed his M.S. degree in May 2014, at the Missouri University of Science and Technology.